Materiales de Construcción
Vol. 74, Issue 353, January-March 2024, e333
ISSN-L: 0465-2746
https://doi.org/10.3989/mc.2024.354623

Shear strength and microstructural investigation on high-volume fly ash self-compacting concrete containing recycled concrete aggregates and coal bottom ash

A. Meena, N. Singh, S.P. Singh ✉

Department of Civil Engineering, National Institute of Technology (Jalandhar, India)
✉: spsingh@nitj.ac.in

Received 24 April 2023
Accepted 08 August 2023
Available on line 13 March 2024

ABSTRACT: This article presents the experimental outcomes of the shear strength and microstructural characteristics of high-volume fly ash self-compacting concrete (HVFYA-SCC) containing recycled concrete aggregates and coal bottom ash as partial replacements for natural coarse aggregates and natural fine aggregates. A total of ten numbers of mixes were produced, including HVFYA-SCC made without recycled concrete aggregates and coal bottom ash (as control) along with HVFYA-SCC mixes made with recycled concrete aggregates (from 25% to 50%) and coal bottom ash (from 10% to 30%). The compressive and shear strength of the HVFYA-SCC mixes were improved by 7% and 4%, respectively, with the incorporation of 20% coal bottom ash and 25% recycled concrete aggregates after 120 days of curing. On the other hand, scanning electron microscopic analysis revealed that incorporating coal bottom ash exhibited the pozzolanic reactions with fly ash densified the binder-aggregate matrix of the resulting HVFYA-SCC.

KEY WORDS: High volume fly ash self-compacting concrete; Coal bottom ash; Shear strength; Recycled concrete aggregates; Microstructural characteristics.

Citation/Citar como: Meena A, Singh N, Singh SP. 2024. Shear strength and microstructural investigation on high-volume fly ash self-compacting concrete containing recycled concrete aggregates and coal bottom ash. Mater. Construcc. 74(353):e333. https://doi.org/10.3989/mc.2024.354623.

RESUMEN: *Resistencia a cortante e investigación microestructural de hormigón autocompactante con elevado contenido de cenizas volantes y con áridos de hormigón reciclado y cenizas de fondo.* Este artículo presenta los resultados experimentales de la resistencia a cortante y las características microestructurales del hormigón autocompactante con alto contenido de cenizas volantes (HVFYA-SCC) que contiene áridos de hormigón reciclado y cenizas de fondo procedentes de calderas de carbón como reemplazos parciales de los áridos naturales, gruesos y finos respectivamente. Se produjeron un total de diez mezclas, incluyendo HVFYA-SCC hecho sin áridos de hormigón reciclado y cenizas de fondo (como control) junto con mezclas HVFYA-SCC hechas con áridos de hormigón reciclado (del 25% al 50%) y cenizas de fondo de carbón (del 10% al 30%). La resistencia a la compresión y a cortante de las mezclas HVFYA-SCC mejoró en un 7 % y un 4 %, respectivamente, con la incorporación de un 20 % de ceniza de fondo y un 25 % de áridos de hormigón reciclado tras 120 días de curado. Por otro lado, el análisis con microscopía electrónica de barrido reveló que la incorporación de cenizas de fondo exhibió reacciones puzolánicas con cenizas volantes que densificaron la matriz de aglutinante-árido del HVFYA-SCC resultante.

PALABRAS CLAVE: Hormigón autocompactante con elevado volumen de cenizas volantes; Cenizas de fondo; Resistencia a cortante; Áridos de hormigón reciclado; Características microestructurales.

1. INTRODUCTION

The Central Electricity Authority of India reported that thermal power plants in India generated around 232 million tons of ash, including fly ash (FYA) and coal bottom ash (BA), in 2020-2021 (1). As per the reports, the country still has 1,738 million tons of ash despite many attempts to utilize it effectively. Moreover, it is anticipated that 60 million tons of river sand will be used annually for construction in metropolitan India (1, 2). This has made India one of the top countries where illegal sand mining is a crucial environmental issue, resulting in the degradation of wetland ecosystems and the disturbance of natural river flows (2, 3).

Similarly recent increase in construction and demolition wastes can be attributed to the renovation of existing buildings, the construction of new buildings in congested cities, and the demolition of ageing concrete structures (4). As infrastructure development continues to grow in developing countries like China and India, there is an increasing demand for the primary ingredients of concrete, including cement, natural fine aggregates (NFA), and natural coarse aggregates (NCA). This surge in demand raises concerns about running out of natural resources and disposing of industrial waste (5). Therefore, finding substitutes for concrete primary components or other ways to make buildings more sustainable is essential. However, incorporating recycled concrete aggregates (RCA) up to 40% in normally vibrated concrete (NVC) mixes can result in a lower environmental impact than the conventional concrete without compromising the performance of the concrete (6).

Similarly, incorporating BA up to 25% in NVC can improve workability and reduce water demand, but higher levels of BA may reduce the compressive strength of the concrete (7). Replacing up to 30% of the NFA with BA in concrete paving blocks can improve their mechanical properties and reduce their environmental impact (8). So, from the literature, it has been concluded that these wastes have some beneficial aspects as a replacement to the naturally available material like NFA and NCA.

Cement manufacturing is accountable for 7.4% of all CO_2 emissions and contributes to global warming issues (9–12). FYA is a fine material in the flue gas that coal-fired thermal power plants produce. FYA not only reduces the amount of cement used, but it also helps to improve the properties of the concrete (13). According to recent studies, concrete can be excellent in strength and durability when cement replacement levels are higher, even up to 75% (13, 14). Using more FYA in concrete will divert more waste from the solid waste stream, and less will end up in landfills. A possible environmentally friendly solution is high volume fly ash concrete (HVFYAC), in which at least 30% of the cement is substituted with FYA (15, 16). Self-Compacting Concrete (SCC) is now the maximum utilized kind of concrete because it is highly workable and can cover enormous amounts of formwork (4, 17). Kapoor et al. conducted an experiment where HVFYA-SCC mixes were created by replacing various percentages of NFA with fine RCA, while coarse RCA was used to replace 100% NCA. The results showed that replacing NFA with fine RCA up to 25% resulted in enhanced compressive strength after 28 and 120 days. However, scanning electron microscopy (SEM) analysis revealed the presence of micropores in the SCC concrete mix, which led to increased permeability. On the other hand, the incorporation of MK as a filler had a beneficial effect, leading to a denser microstructure (18). Similarly, Singh and Singh (19) conducted a study where HVFYA-SCC mixes were investigated. In their experiment, 50% and 100% of NFA were replaced with fine RCA, while 100% NCA was substituted with coarse RCA. The results showed that the compressive strength of HVFYA-SCC mixes made with RFA decreased compared to the control mix. However, the inclusion of MK in HVFYA-SCC mixes containing RFA helped offset the loss of compressive strength resulting from the substitution of NFA with RFA. A greater reduction in compressive strength was observed in HVFYA-SCC mixes where both NCA and RFA were fully replaced with RCA. The findings from SEM and XRD analysis supported these trends, confirming the differences in microstructural and crystallization behavior among the different concrete mixes. The HVFYA-SCC mix incorporating metakaolin and 50% fine RCA exhibited the formation of overlapped CSH layers at 28 days, dense CSH blocks at 90 days, and a lower presence of crystalline $CaCO_3$. These observations help explain the superior performance of this mix compared to the others.

The concrete industry has recently emphasized producing sustainable SCC, replacing cement and NFA with alternate solutions like FYA and BA (20). BA is similar in size to NFA and has emerged as the most feasible choice among available options.

Replacing NFA with BA at acceptable amounts (up to 20%) can enhance the mechanical and durability performance of NVC and SCC, and its use in concrete at a later stage offers more pozzolanic advantages (15, 21). Nevertheless, the mechanical and durability characteristics of concrete mixes containing BA and RCA significantly degrade compared to base SCC (22–24). For the past two decades, researchers have extensively studied the fresh and mechanical properties of HVFYA-SCC with partial replacement of RCA and BA (15, 20). In general, the shear transfer across cracks plays an important role in determining the shear strength of concrete structures. The aggregates interlock effect is a crucial mechanism for shear transfer across cracks, and it is influenced by various reasons such as the crack width, strength of concrete, stiffness of the lateral

constraint etc., (25). It is worthwhile to mention here that incorporating RCA may impact the aggregate interlock and shear transfer capabilities of concrete. The investigations conducted by Waseem and Singh (2016) and Rahal (2017) confirmed that the use of more amount of RCA per unit volume with weak surrounding mortar imparts an important influence on the interlocking and shear transfer capabilities of concrete (26, 27). Likewise, the shear behavior of HVFYAC containing 50% FYA was studied by Li et al. (2022) (28). The conclusions of these investigations are oriented toward the prominence of HVFYAC over conventional concrete.

Furthermore, studies have shown that incorporating RCA impacts the shear strength of concrete. Some studies indicated a decrease in shear strength with RCA on replacing NCA (7% for 20-50% and 28% for complete replacement), while few resulted in a marginal increase in shear strength (29). In comparison, HVFYAC showed superior shear strength compared to conventional concrete. Using sustainable concrete made of 50% FYA and 50% RCA showed an average shear capacity 10% lower than traditional concrete and lower than concrete with 50% FYA or 50% RCA (30). These studies provide insights into the potential use of RCA and sustainable concrete in structural applications.

It has been noted from the existing literature that considerable investigations indicate the successful feasibility of utilizing various industrial wastes (particularly FYA, BA and RCA) in different forms of NVC and SCC. It has also been important to mention here that failure of concretes due to the occurrence of shear loading is sudden and also catastrophic (31, 32). On the other hand, no special provisions are available in the design shear strength of HVFYA-SCC to cope with such failure losses. Hence, the experimental study has been planned to determine the effects of replacing RCA and BA with NCA and NFA, respectively, on the shear strength performance of HVFYA-SCC. The microstructural characters were also planned to examine in support of the preceding strength feature.

To attain in-depth knowledge of shear cracks aspects/behavior, the ultimate aim of the current investigation was to fulfill the aforesaid gap by conducting direct shear strength tests on various combinations of HVFYA-SCC. In addition to the preceding, the compressive strength performance was also estimated for general comparison. The attained experimental outcomes were finally corroborated by investigating microstructural changes with the support of FTIR, XRD and SEM techniques. Eventually, the proposed aim further follows the approach for the maximum utilization of industrial waste products in manufacturing sustainable forms of HVFYA-SCC. Since the said approach conserves vital natural resources, it substantially reduces the number of abovementioned wastes in preceding paragraphs that are generally being impelled towards landfills for their idle disposal (33–39). Therefore, the outcomes of this study will indicate valuable information on the performance and potential benefits of using HVFYA-SCC in advanced structural designs and construction. The findings will also support its implementation as a sustainable and environmentally-friendly alternative to conventional concrete(s).

Furthermore, the present study has investigated the effect of FYA (70%) and BA (10-30%) at higher replacement levels. To the best of authors' knowledge, no other existing study has considered the effect of high-volume fly ash (70%) as a cement replacement along with BA (10-30%) as NFA replacement and RCA (0-50%) as NCA replacement in SCC. The outcomes of the current experimental investigation indicate substantial variation (s) in shear and compressive strength of the developed concrete covering the existing gap in available literature. In fact, the present investigation is an attempt to achieve three-way benefit by minimising the dependency of concrete on cement by efficient utilisation of HYFYA-SCC; minimising natural resource depletion by utilisation of BA and RCA as aggregates replacement and encouraging clean and green production in construction industry.

2. EXPERIMENTAL PROCEDURES

2.1. Materials

In this investigation, OPC 43-grade, FYA Class-F, NFA (river sand of 4.75 mm), BA (4.75 mm), NCA (maximum 12.5 mm size) and RCA (maximum 12.5 mm) were used for the making of HVFYA-SCC. In this study, OPC and FYA agreed to IS 8112:2013 (40) and ASTM C618 (41), respectively. The physical characteristics of OPC are presented in Table 1. The specific gravity of BA and FYA are 2.09 and 2.10 respectively. The chemical composition of OPC, BA and FYA are presented in Table 2. The SEM image of the particles OPC and FYA are shown in Figures 1 (a) and 1 (b), likewise indicating that the OPC particles are angular in shape, and the FYA are smooth and spherical. OPC was procured from the ACC cement manufacturing plant at Ropar, India. FYA was collected from the Nabha power plant in Rajpura, India. NFA and NCA were collected from Trehti quarry at Pathankot, India. NFA was used in the present study as per code IS 383-2016 (42), and the NFA was found to be retained in Zone II by carrying out sieve analysis as per the specification of IS 383-2016 (42). BA replaced the NFA at 0%, 10%, 20%, and 30% collected from a Ropar thermal power plant in India. Figure 2 shows the particle size gradation of different ingredients. Figure 3 (a-d) illustrates the pictorial view and the SEM image of NFA and BA, respectively. Moreover, BA ranged in Zone II as per IS 383-2016 (42).

Table 1. Physical properties of OPC.

Properties	**Test result**	**Requirement as per IS 269: 2015** (104)	**Remarks**
Specific gravity	3.15	-	Performed by the Authors' Institute in Material Testing Laboratory
Setting time (minutes)			
(i) Initial setting time	62	Min. 30	
(ii) Final setting time	270	Max. 600	
Soundness (mm)			
(i) By Le-Chatelier Method	1.00	Max. 10	
Compressive strength (MPa) for mortar specimens as per IS 4031:1988 (Part 6) (105)			
(i) 3 Days (72 ± 1 h)	24.6	23	
(ii) 7 Days (168 ± 2 h)	34.3	33	
(iii) 28 Days (672 ± 4 h)	45.2	43	

Table 2. Chemical composition of OPC, BA and FYA.

Chemical composition (% weight)	**OPC**	**BA**	**FYA**
CaO	60.58	0.78	1.43
Fe_2O_3	3.99	8.31	5.01
SO_3	2.83	0.21	0.22
Al_2O_3	5.88	29.13	26.92
K_2O	1.12	1.27	1.31
SiO_2	20.89	56.4	60.57
TiO_2	0.22	0.22	1.69
MgO	0.93	0.42	0.83
Na_2O	0.81	0.07	0.12
Loss of Ignition	2.01	0.87	1.82

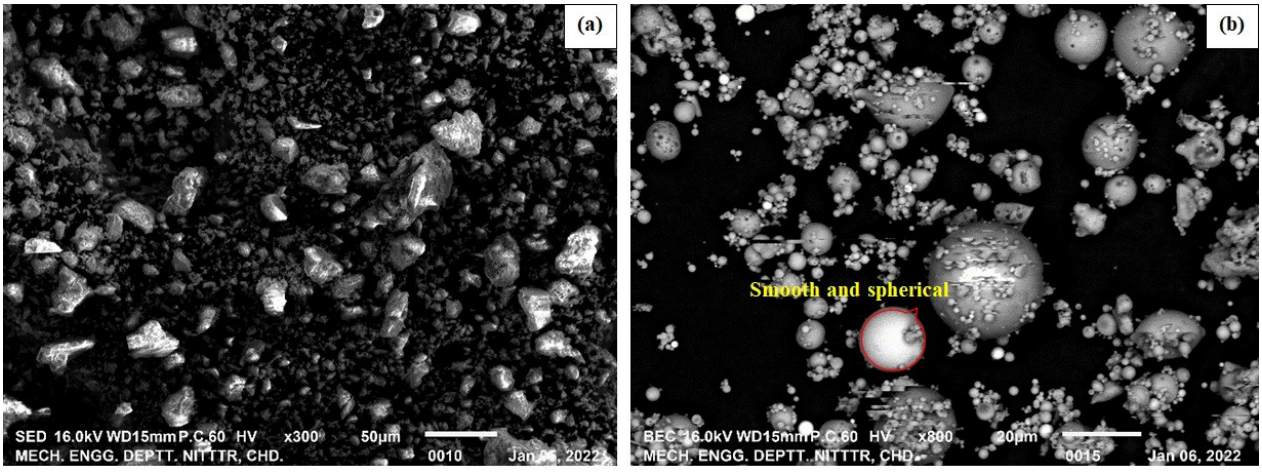

Figure 1. SEM images: (a) OPC, (b) FYA.

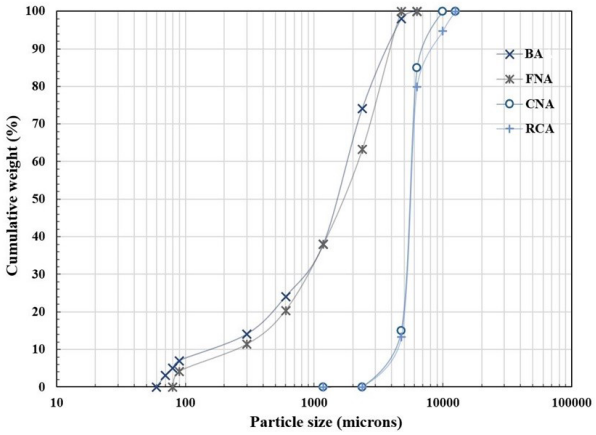

Figure 2. Gradation curve of aggregates and BA.

The NCA were used in the proportion of 25%, 42% and 33%, respectively, for 6.36 mm, 10 mm and 12.5 mm in saturated surface dry (SSD) conditions. The NCA was replaced with RCA at 0%, 25% and 50%, and to get RCA, the tested concrete specimens were crushed and sieved as per IRC:121-2017 (43) in Structures Testing Laboratory of the authors Institute. The physical properties of NFA, BA, NCA and RCA are presented in Table 3. Figure 3 (e-f) represents the pictorial view of the NCA and RCA used in this investigation respectively. However, it is worthwhile to mention that in the current investigation the authors have used weigh batching approach instead of equivalent volume batching approach for the mix design. Similar approach has been successfully implemented in significant number of investigations as available in literature (23, 44, 45). Moreover, the authors have incorporated only selected amount of RCA (maximum 50%) and BA (maximum 30%) in comparison to the investigations wherein the effect of density has been considered for the higher amount of RCA (>50%) and BA (>30%) (18, 20, 46–49). Since the amount of altered ingredients was less and the source of procurement was not changed during entire investigation therefore for the same reason the authors have not considered the effect of variation of density of BA and RCA in the current study. A high-range water reducer superplasticizer (SP) of MasterGlenium 51 (polycarboxylic ether-based) was utilized in different doses by weight of the binder to attain the desired HVFYA-SCC, confirming IS 9103 (50).

Table 3. Physical properties of BA, RCA, NFA and NCA.

Properties	BA	RCA	NFA	NCA
Water absorption (%)	30	5.65	1.2	0.68
Fineness modulus	1.52	6.8	3.98	6.9
Specific gravity	2.09	2.44	2.75	2.64

Figure 3. Materials used in this study.

2.2. Mixtures

For the research, ten HVFYA-SCC mixes with a consistent binder content of 688 kg/m^3 and a water to binder proportion of 0.25 were made. NFA and NCA additions of 887 kg/m^3 and 711 kg/m^3, correspondingly, were made. Out of ten HVFYA-SCC mixes, one control mix (CF70B0-R0) was prepared with 30% OPC and 70% FYA combining 100% NFA and 100% NCA. The remaining mixes were made using various substitutions, such as replacing NCA with 25% and 50% RCA and NFA with 10%, 20%, and 30% BA. The mix proportions for all the HVFYA-SCC mixes are revealed in Table 4. It is worthwhile to mention here that, the water absorption of both RCA and BA has higher values in comparison to that of NCA and NFA. The absorption factor was duly considered while preparation of all SCC mixes. The RCA were incorporated in surface saturated dry condition while additional water was added at the time of mixing of all HVFA-SCC mixes due to higher absorption of BA particles. The HVFYA-SCC mixes were prepared according to European federation of national associations representing concrete (EFNARC; 2005) (51) guidelines, and SP was incorporated in different proportions ranging from 0.65% to 1.38% by weight of the binder.

Table 4. Details mix proportions of HVFYA-SCC mixes in kg/m³.

S no	Mix identity	OPC	FYA	NFA	BA	NCA	RCA	Water	SP
1	CF70B0-R0 (Control)	206.4	481.6	887	0	711	0	170	4.47
2	CF70B10-R0	206.4	481.6	798.3	88.7	711	0	170	5.16
3	CF70B10-R25	206.4	481.6	798.3	88.7	533.25	177.75	170	5.85
4	CF70B10-R50	206.4	481.6	798.3	88.7	355.50	355.50	170	6.19
5	CF70B20-R0	206.4	481.6	709.6	177.4	711	0	170	6.88
6	CF70B20-R25	206.4	481.6	709.6	177.4	533.25	177.75	170	7.57
7	CF70B20-R50	206.4	481.6	709.6	177.4	355.50	355.50	170	7.91
8	CF70B30-R0	206.4	481.6	620.9	266.1	711	0	170	8.26
9	CF70B30-R25	206.4	481.6	620.9	266.1	533.25	177.75	170	8.94
10	CF70B30-R50	206.4	481.6	620.9	266.1	355.50	355.50	170	9.49

2.3. Experimental methodology

2.3.1. Workability and compressive strength

HVYFA-SCC mixes were evaluated for their workability through various tests such as slump flow, V-funnel, and T_{500} as per the EFNARC 2005 standard (51). To ascertain the compressive strength of all HVFYA-SCC mixes, tests were performed in accordance with Indian Standard (IS) 516-2021 (52). Cubic specimens measuring 100 mm x 100 mm x 100 mm were produced and tested for compression using a 2000 kN capacity compression testing machine (CTM). The tests were conducted after 28 and 120 days of curing with a constant loading rate of 2.5 kN/s.

2.3.2. Direct shear strength

Direct shear strength of HVFYA-SCC mixes was tested as per method recommended by Bairagi and Modhera (53). Two plates of light steel (150 x 85 x 10 mm and 150 x 110 x 10 mm) and two bars (12 mm and 22 mm in diameter) were utilized to carry out the test on a CTM. Plates were positioned on top of the L-shaped specimen, and a 22 mm dia. rod was placed together to the plate as presented in Figure 4 (a). The specimen was tested for accuracy and reliability at 7, 28, 56, 90, and 120 days using a 2000 kN CTM at a 2.1 kN/sec loading rate (Figure 4).

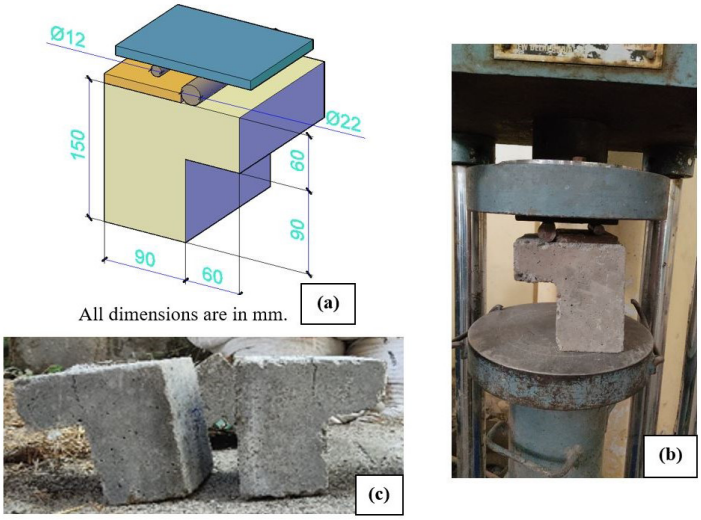

Figure 4. (a) Design of specimen for shear strength, (b) testing arrangement, (c) tested specimens.

2.3.3. Microstructural analysis

The chemical and microstructural characteristics of the HVFYA-SCC mixes were examined using X-ray diffraction (XRD), scanning electron microscopy (SEM), and Fourier transform infrared spectroscopy (FTIR) analyses. The Bruker Tensor 27 instrument was used for FTIR analysis of HVFYA-SCC powder specimens, scanning the range of 400-4000 cm-1 to identify molecular groups. Powder specimens under 90 microns were obtained through crushing and grinding techniques of 100 mm cube specimens for testing. The specimens were examined utilizing FTIR analysis after 120 days. The Panalytical Empyrean XRD apparatus was used to identify mineral phases in HVFYA-SCC powder specimens for XRD analysis. The specimens used for XRD analysis were similar to those used for FTIR analysis. XRD analysis was performed on the specimens after 120 days of curing, collecting data from an angle of 2θ between 10° and 70° in 0.02° increments, and analyzing it with the X'pert high score plus software (54). The microstructure of the produced HVFYA-SSC specimens was described using SEM analysis. SEM analysis of a broken concrete specimen from a 100 mm cube specimen was conducted using a ZEISS Sigma 500 VP field emission scanning electron microscope after 120 days of curing.

3. RESULTS AND DISCUSSIONS

3.1. Workability and compressive strength

Figure 5(a) shows the difference in slump flow and T_{500} time, where the estimated value of slump flow diameter was between 710-745 mm. This value is categorized under the SF2 class ranging from 660-750 mm as per EFNARC 2005 (51). Adding BA and RCA decreased the slump flow value, but adding an equivalent amount of SP dosage can prevent it. The results indicate that adding 30% BA negatively affected the slump values, while the mix with 50% RCA had the highest reduction (almost 4%) with reference to control HVFYA-SCC mix. Filling ability of HVFYA-SCC mixes was evaluated using T_{500} time, which ranged from 3.3 to 4.8 seconds. Figure 5(b) indicates that the T_{500} time increased with an increase in the amount of BA and RCA. Singh et al. (55) also observed a decrease in flow ability at substitution levels of 10% BA and 50% RCA for NFA and NCA, correspondingly. The control HVFYA-SCC mix (CF70B0-R0) had the minimum T_{500} time, while the highest value was observed for the CF70B30-R50 mix. (15, 20).

Figure 5(b) indicates the difference in V-funnel time value and SP dosages, with RCA and BA containing HVFYA-SCC mixes having a better V-funnel time value as compared to control mix (CF70B0-R0). Alike results were described by Singh et al. (55) when studying the use of BA and RCA as a substitution for NFA and NCA, respectively. The V-funnel value for all HVFYA-SCC mixes ranged from 6-13.5 seconds. The mixes CF70B0-R0, CF70B10-R0, and CF70B10-R25 were categorized under the VF1 (0-8 seconds) viscosity class, while the VF2 (9-25 seconds) viscosity class included the CF70B10-R50, CF70B20-R0, CF70B20-R25, CF70B20-R50, CF70B30-R0, CF70B30-R25, and CF70B30-R50 mixes. Also, the results revealed that the variation in J ring spread, where the estimated value of flow diameter was between 700-740 mm (Figure 5(c)). All the mixes met the EFNARC 2005 (51) limit with blocking ratios between 0.92 and 0.98 (Figure 5(d)). The irregularly shaped porous particles of BA and the rough texture adhering mortar on RCA may have combined effects that reduce the passage ability of the mixes by increasing inter-particle friction and obstructing concrete flowability (56–58).

Figure 6 (a) indicates that higher BA content led to lower compressive strength at 28 days. The reduction was highest for the mix with the lowest BA content (CF70B10-R0), showing a decrease of 18%. However, for mixes with larger amounts of BA (20% and 30%), the decrease in compressive strength was

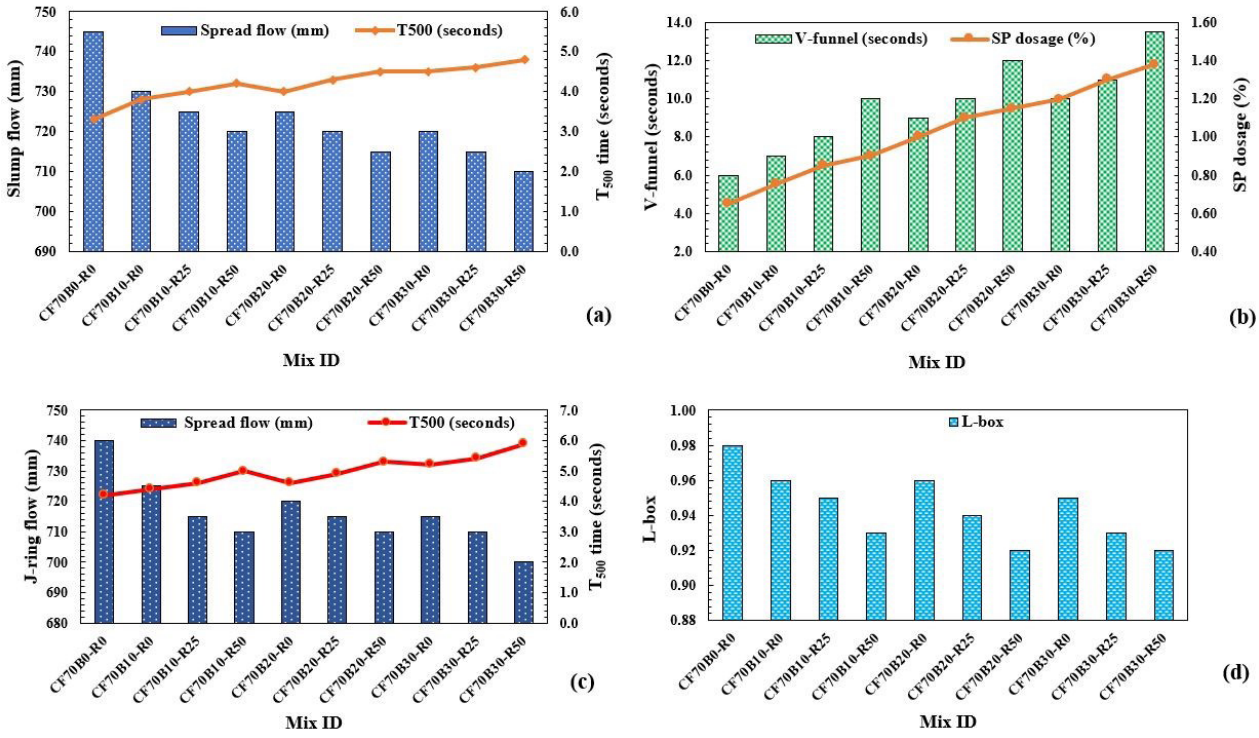

Figure 5. (a) Slump flow and T_{500} time of HVFYA-SCC mixes, (b) V-funnel and SP dosage of HVFYA-SCC mixes, (c) J-ring flow and T_{500} time of HVFYA-SCC mixes, (d) L-box of HVFYA-SCC mixes.

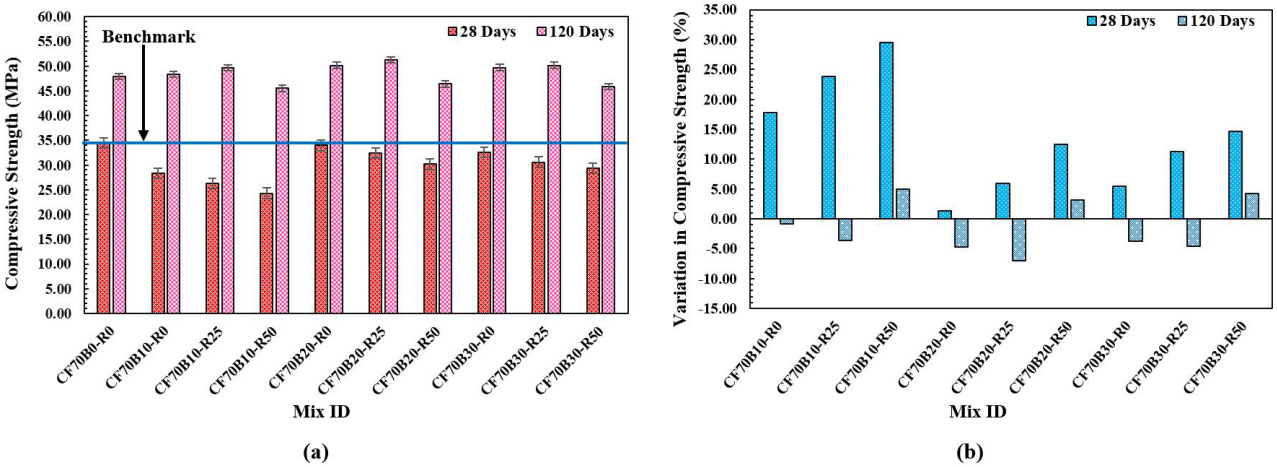

Figure 6. (a) Compressive strength of HVFYA-SCC mixes, (b) Variation of compressive strength relative to control mix (CF70B0-R0).

only 5% with reference to control HVFYA-SCC mix (Figure 6 (b)). Similarly, Figure 6 (b) illustrates those mixes containing 10% BA exhibited an increase in compressive strength after 120 days. Previous studies (32, 58) suggest that HVFYA and BA in the mixes induce pozzolanic action at longer curing ages, which may explain the improved behavior.

After 28 days, the CF70B10-R25 and CF70B10-R50 mixes, which contained 10% BA and 25% and 50% RCA, exhibited lower compressive strength with reference to control HVFYA-SCC mix, with reductions of 24% and 29%, respectively At 120 days, the mix with 25% RCA demonstrated a slight improvement in compressive strength with reference to control HVFYA-SCC mix, which may be attributed to the presence of BA and FYA, resulting in additional pozzolanic reactions (15). The primary pozzolanic activity due to presence of FYA and BA has been explained in context to their chemical properties in which action due to pozzolanicity of CaO and SiO_2 mainly has been happened. It is worthwhile to mention here that BA has been incorporated in place of NFA with constricted amount up to 30% in preparation of HVFA-SCC mixes. Herein, as mentioned earlier the pozzolanic action of BA comes into picture at later ages and that too with less impact in comparison to that of FYA. Further it was inferred that the reactive SiO_2 is the chief parameter which strongly influences the Na_2O content as present in coal fly ashes (59, 60). The stronger influence of SiO_2 due to higher amount (60.57%in FYA) and presence of Na_2O leads to development of more C-A-S-H gels, consequently improve the strength properties of the HVFA-SCC mixes (60–62). Similar influence of K_2O has been noted wherein pozzolanic action has supplemented the strength aspects in concrete (59, 63, 64).

Conversely, the compressive strength of the CF70B10-R50 mix, containing 50% RCA, declined with increasing curing time, likely due to the presence of aged, adhered mortar in the RCA that deteriorated its structural properties (65). In contrast, the CF70B20-R25 and CF70B30-R25 mixes, containing 20% and 30% BA and 25% RCA, exhibited compressive strengths 7% and 4% higher than the control mix after 120 days, as shown in Figure 6(b). The enhancement in compressive strength can be attributed to the additional development of C-S-H during later stages of curing, which resulted from the pozzolanic reaction of BA and FYA (32, 58). Nonetheless, the frail interface transition zone (ITZ) between the adhering mortar and the porous aggregates might lead to a slight reduction in compressive strength when replacing 50% of RCA in comparison to 25% in all formulated mixes (58, 65).

In the current investigation the chemical analysis indicates higher amount of CaO and SiO_2 for FYA (1.43% and 60.57%) compared to that of BA 0.78% and 56.4%) respectively. Also, the particle size of FYA is much finer than that of BA particles consequent in higher reactivity of the former than reactivity of the later. In fact, the higher amount of aforesaid compounds generally results in improvement of the HVFA-SCC mixes due to additional pozzolanic reactions thereby increasing the heat of hydration. Moreover, the amount of CaO and SiO_2 for FYA and BA mostly depends on the source and type of coal or the parent material (15, 46). In India, due to bituminous type of coal (66), Class F type FYA is present along with lower grade of BA. Hence due to this reason the pozzolanic action of FYA is more in comparison to BA used in this investigation.

3.2. Direct shear strength

Figure 7(a) displays the direct shear strength results for all the HVFYA-SCC mixes after 7-days

periods of curing. The data showed a general decline in direct shear strength as the BA concentration increased. Figure 7(b) further revealed a decrement of 5%, 1%, and 3% for HVFYA-SCC mixes CF70B10-R0, CF70B20-R0, and CF70B30-R0, correspondingly, reference to the control HVFYA-SCC mix. This pattern was too observed for shear strength at 28 and 56 days. The decrease in HVFYA-SCC mixes during the early stages of curing was due to the decline in heat of hydration of cement and pozzolanic activity of FYA and BA (24, 67). However, after 90 days, the shear strength of the HVFYA-SCC mixes was observed to be comparable to the HVFYA-control mix. The shear strength of HVFYA-SCC mixes with varying amounts of BA and curing time was analyzed in Figure 7(b). The results showed that CF70B10-R0, CF70B20-R0, and CF70B30-R0 mixes had a slight increase of up to 2% in shear strength than the control mix. The same trend was observed for mixes with 10% to 30% BA, where shear strength increased with curing time up to 120 days. On the other hand, when 25% and 50% RCA were added to the 10% BA mixes, a decrease in shear strength was observed with reference to control HVFYA-SCC mix. Specifically, the shear strength at 7 days dropped from 3.57 MPa for the CF70B0-R0 mix to 3.23 MPa and 3.11 MPa, respectively, when 25% and 50% of the RCA were replaced. HVFYA-SCC mixes with 20% and 30% BA showed a decrease in shear strength as curing increased up to 56 days.

Furthermore, after 90 days curing age, the shear strength of the control mix (CF70B0-R0) improved slightly from 6.45 MPa to 6.54 MPa with 25% replacement of RCA. BA and FYA may increase direct shear strength in HVFYA-SCC with lower RCA concentrations due to additional pozzolanic reactivity (15, 32). However, 50% RCA had the contrary effect, the shear strength of CF70B10-R50 decreased up to 1% after 90 days of curing. The weak adhered mortar in RCA leads to a reduction in over-all shear strength, which could be attributed to the maximum RCA content and poor structural properties (65, 68). Mixes with 20% and 30% BA showed similar trends, where extended curing time resulted in higher direct shear strength when 25% RCA was used as a replacement for NCA, while 50% RCA replacement resulted in reduced shear strength. The shear strength of the CF70B20-R25 mix improved from 3.49 MPa at 7 days of curing to 7.21 MPa at 120 days. As per the results, the CF70B20-R25 mix had higher strength than the control mix at 120 days periods of curing (7.00 MPa). Similarly, mix CF70B30-R25 exhibited 2% higher compressive strength after 120 days periods of curing with reference to control mix as depicted in Figure 7 (b).

Overall, the study revealed that the shear strength of 20% BA-based mix (CF70B20-R25) was significantly increased with the use of 25% RCA. This was in contrast to mixes with 10% and 30% replacement levels of BA with NFA. The increase in direct shear strength was more evident during later curing periods, where the mix CF70B20-R25 showed 2% lower shear strength than the control mix after 7 days, but significantly increased to 7.21 MPa after 120 days than the control mix (7.00 MPa). This rise in strength at later curing period was attributed to the pozzolanic effect of BA and FYA, which produced more C-S-H. Moreover, the interlocking nature of the aggregates was improved by the physical interface of fine BA with an irregular shape and sharp edge, making them more resistant to shear stress transferred during deformation (32, 58, 69).

Figure 8 (a), observed that the plane of failure is vertical i.e., just under the application of loading bar which represents the failure under pure shear failure along a single plane. However, Figure 8 (b), showed the failed specimens most of specimens failed due to breakage/splitting of coarse aggregates instead of failure of aggregate-matrix interface and even some of the RCA failed in the same manner which further

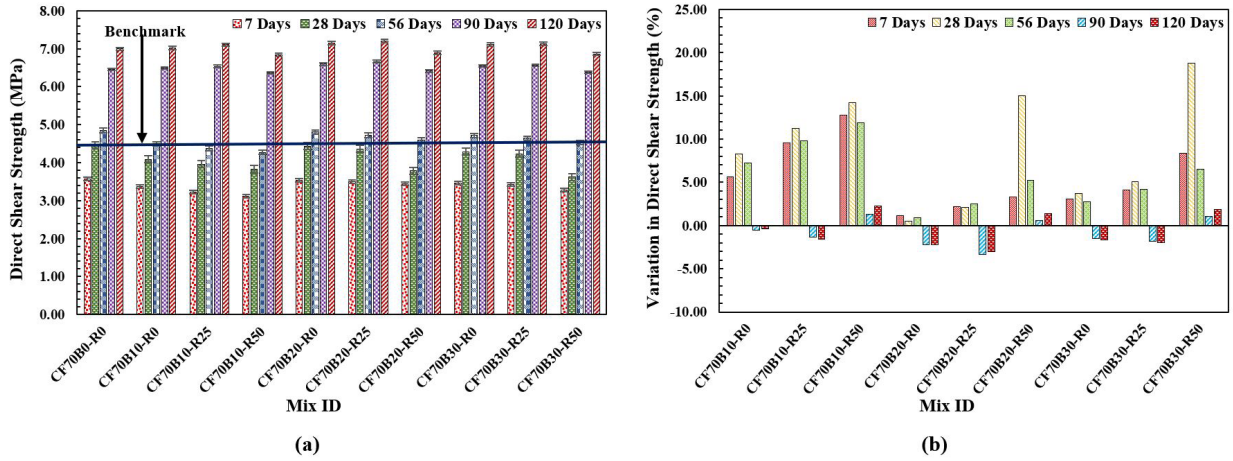

Figure 7. (a) Direct shear strength of HVFYA-SCC mixes, (b) Variation of direct shear strength relative to control mix (CF70B0-R0).

increase the shear capacity due to denseness of matrix (25, 26). In contrast, the addition of 50% RCA as a NCA leads to a significant reduction in direct shear strength for all BA mixes, including CF70B10-R50, CF70B20-R50, and C750B30-R50, at different curing ages, which is much lesser than the control mix (CF70B0-R0). After 120 days curing, the direct shear strengths of HVFYA-SCC mixes that contained 50% RCA, such as CF70B10-R50, CF70B20-R50, and CF70B30-R50, were measured at 6.84 MPa, 6.90 MPa, and 6.86 MPa correspondingly, then the control HVFYA-SCC mix (7.00 MPa). The reduced direct shear strength can be attributed to the presence of old, residual adhering mortar in RCA, which contributes to the poor structural characteristics of materials at higher RCA content levels (65, 68).

3.3. Microstructural analysis

3.3.1. X-ray diffraction analysis

Herein the effect of addition of BA primarily in HVFYA-SCC mixes has been discussed. It has also been observed that with addition of BA in HVFYA-SCC mixes an ample variation in the counts of peaks of different compounds [such as Portlandite (P), calcium silicate hydrate (C-S-H), quartz (Q), calcium silicate (CS) and, gismondine (CASH)] has been noticed. In fact, all the HVFYA-SCC mixes have been compared with the control HVFYA-SCC (CF70B0-R0) mix. The additional peaks which are not participating in enhancing the performance of HVFYA- SCC mixes have not been discussed. XRD analysis results after 28 and 120 curing days, are presented in Figures 9-10. The following mineral phases were identified by XRD in all HVFYA-SCC mixes: Portlandite (P), calcium silicate hydrate (C-S-H), quartz (Q), calcium silicate (CS) and, gismondine (CASH) after 28 and 120 days of curing. Also these mineral phases are prominent in later ages, the pozzolanic reactions occur due to presence FYA and BA primarily in mortar phases (46, 54, 70–72), hence for the same reason the investigation have been made for the current study.

The prominent peaks for P were located at around 29.37° and 50.11° (46, 72–74). For Q, the intensities were observed at 20.84°, 26.66°, 39.52°, 44.64°, 50.16°, 59.94° and 68.13°. Additionally, C-S intensity was located at 33.15°, the greatest intensity peaks of C-S-H were detected at 20.84°, 29.37°, 33.15°, 44.64° and 50.11° and for CASH shows 2θ at 20.84°. After 28 days curing stage (Figure 9(a-c)), the BA-based HVFYA-SCC mixes exhibited lower peaks of C-S-H than the HVFYA-SCC mix CF70B0-R0, which might be the decrease in the heat of hydration of cement and slowdown of FYA and BA pozzolanic action throughout the initial periods of curing are the reasons for observed incline in HVFYA-SCC mixes (46).

The mix CF70B20-R0, which predominates the mechanical properties of the concrete matrix, and the most important intensity peaks of C-S-H were found at 29.09° after 120 days of curing. Figure 10(a) re-

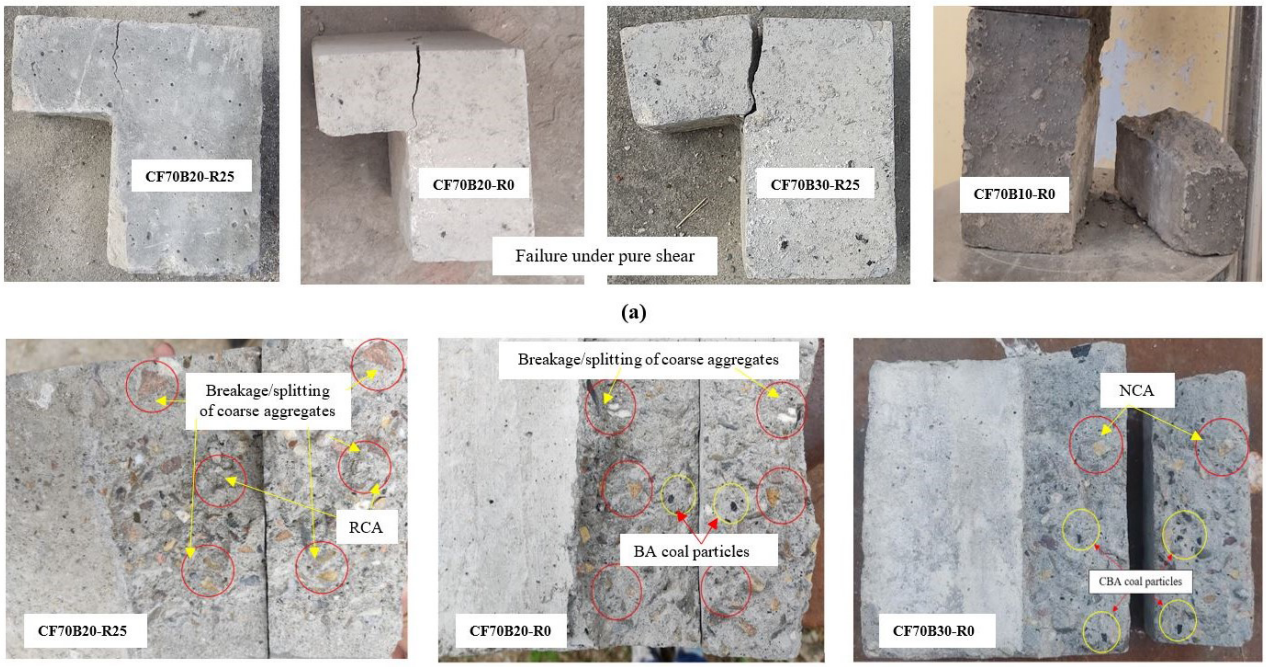

Figure 8. (a) Failure modes of tested specimens, (b) Interface photos after breaking the specimens about cracked plane (manually).

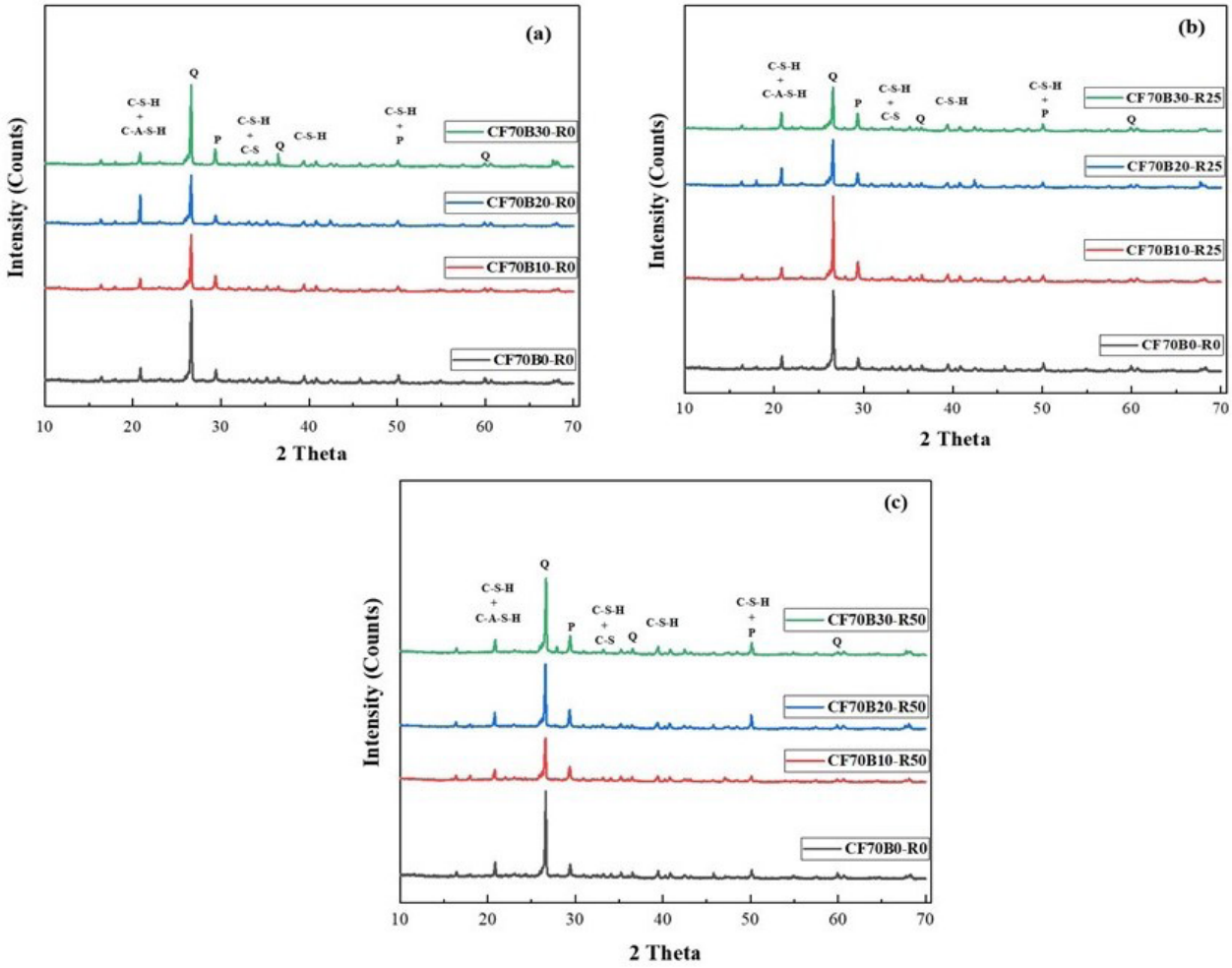

Figure 9. XRD patterns of the HVFYA-SCC mixes with 10-30% BA at 28 days of curing: (a) 0% RCA, (b) 25% RCA and (c) 50% RCA.

vealed that the intensity of C-S-H was more for mix CF70B20-R0 than in other HVFYA-SCC mixes. The trends of C-S-H intensities in the HVFYA-SCC mixes are as follows CF70B20-R0> CF70B30-R0> CF70B30-R0 > CF70B0-R0. Overall, the peaks of P were found to be lower for mix CF70B20-R0, which may be owing to the pozzolanic interaction between the FYA and BA at120 days curing age (75).

Figure 10(b) depicted that the intensity of C-S-H was more for CF70B20-R25. In contrast, the intensity of the hydrated product was lower in other HVFYA-SCC mixes, including the HVFYA-SCC mix CF70B0-R0. The trends of hydrated products were as follows CF70B20-R25> CF70B30-R25> CF70B10-R25 > CF70B0-R0.

Figure 10(c) shows that after 120 days curing periods, the HVFYA-SCC mix CF70B20-R50 has higher hydrated products than the other mixture. Overall, when varying the concentration of RCA, the CF70B20-R25 mix had superior hydrated product intensity supported by mechanical strength. It can be observed that the intensity of peaks P was decreased or gone entirely, particularly in CF70B20-R25 combinations. Moreover, BA pozzolanic response and filler effect in the HVFYA-SCC mix increased strength properties at the optimal dose of 20% BA and 25% RCA content (58, 69). The presence of Pozzolanic materials benefited the process by producing enough hydration products in the shape of C-S-H (54, 70, 71, 76, 77).

3.3.2. Fourier transform infrared spectroscopy

FTIR was used to test concrete mixes for distinctive bands at different wavenumbers. The HVFYA-SCC mix was found to contain diverse molecular groups after 28- and 120-days periods of curing, as shown in Figures 11 (a-c) and 12 (a-c). The 4000 to 500 cm^{-1} wavenumber FTIR spectra revealed the chemical interaction between the cementitious matrix, BA, and FYA.

The transmittance bands at 3753 cm^{-1} represent vibration of the C-H groups produced by silicates in hydrated cement, while the bands at 3357 cm^{-1} represent $Ca(OH)_2$ bonding frequency. As extra C-S-H forms, more $Ca(OH)_2$ consumed (78, 79).

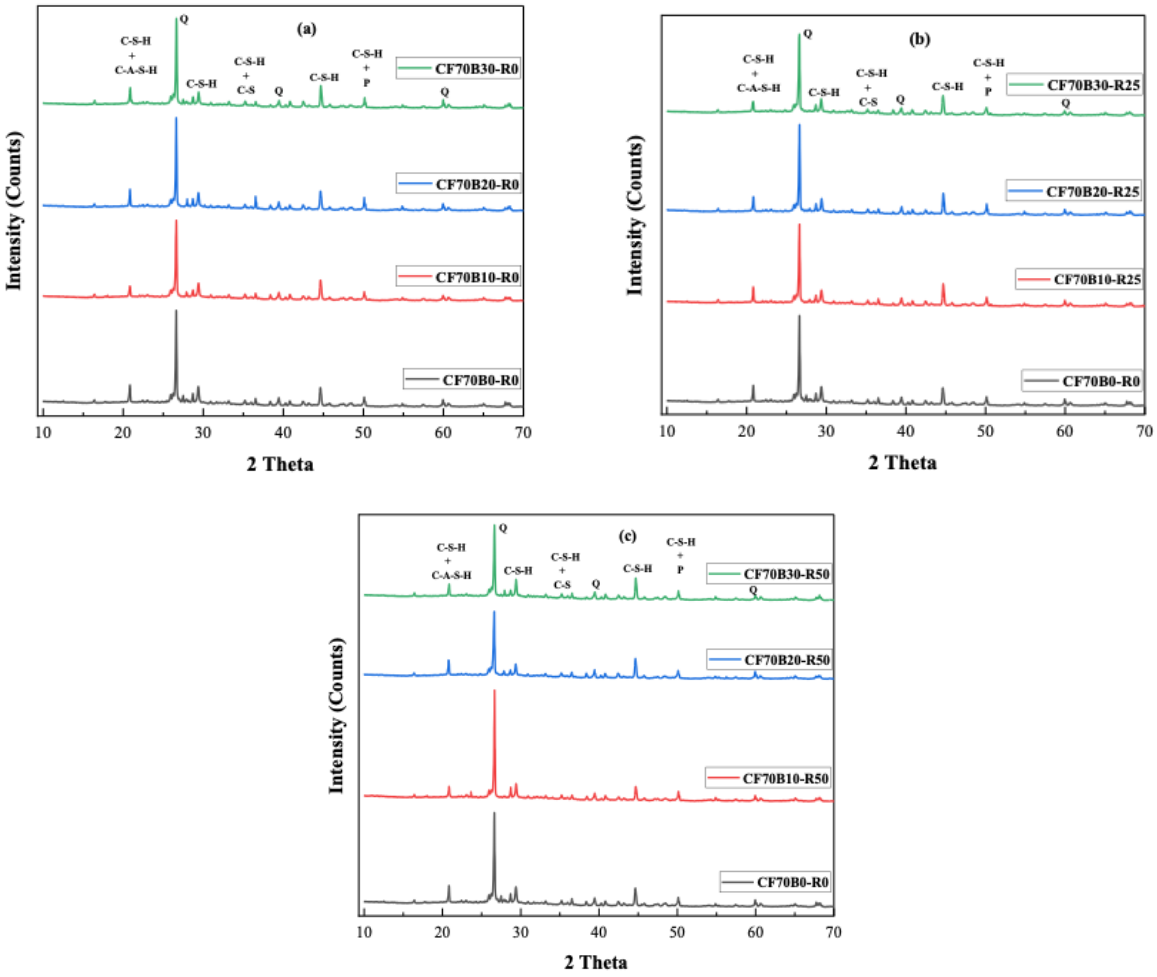

Figure 10. XRD patterns of the HVFYA-SCC mixes with 10-30% BA at 120 days of curing: (a) 0% RCA, (b) 25% RCA and (c) 50% RCA.

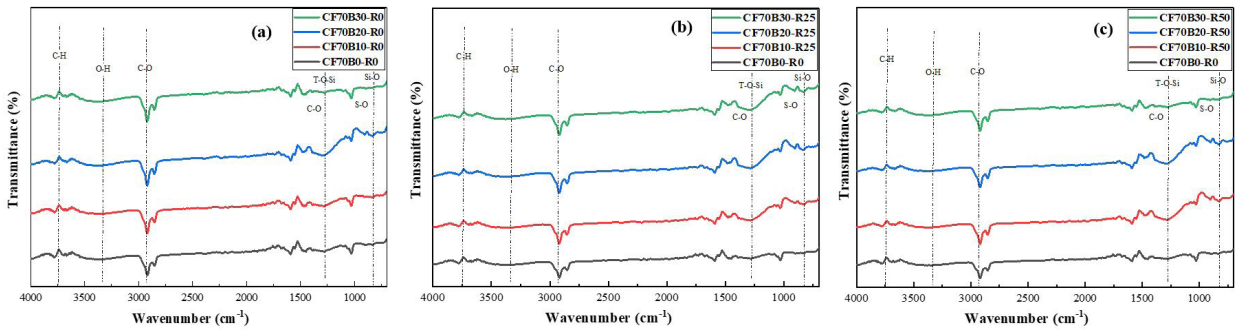

Figure 11. FTIR patterns of the HVFYA-SCC mixes with 10-30% BA at 28 days of curing: (a) 0% RCA, (b) 25% RCA and (c) 50% RCA.

Among the HVFYA-SCC mixes tested, the CF70B20-R25 mix demonstrated the most significant decrease in the O-H group band after 120 days, while CF70B0-R0, CF70B10-R0, and CF70B30-R0 exhibited the least considerable decrease. The BA and FYA compounds in the HVFYA-SCC matrix exhibited higher pozzolanic activity than the HVFYA-SCC mix CF70B0-R0, resulting in formation of more C-S-H at a later stage. In the CF70B10-R25 and CF70B30-R25 mixes, the intensity of O-H groups decreased significantly than HVFYA-SCC mix CF70B0-R0 after 120 days, likely due to $Ca(OH)_2$ consumption by FYA, as shown by XRD results.

Adding an optimal amount of BA in the HVFYA-SCC mixes improved the content of C-S-H, resultant in less free water availability and less $Ca(OH)_2$

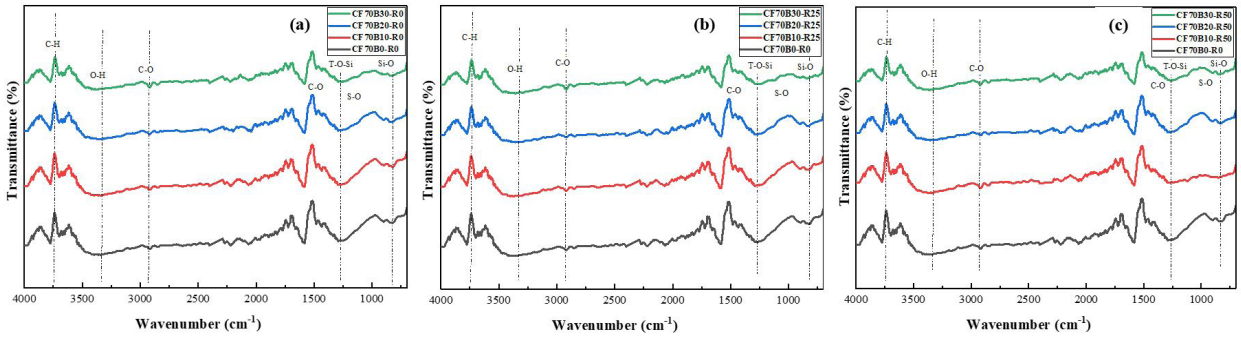

Figure 12. FTIR patterns of the HVFYA-SCC mixes with 10-30% BA at 120 days of curing: (a) 0% RCA, (b) 25% RCA and (c) 50% RCA.

than HVFYA-SCC mix CF70B0-R0. The prominent peaks of 2911 cm^{-1} and 1447 cm^{-1} represent the widening manners of C-O bands of $CaCO_3$ and hydration products (CH), respectively, representing the reaction among $Ca(OH)_2$ and CO_2. The absorbance of the H-O-H band at 1567 cm^{-1} is recognized as a water bond (54, 80), and the widening absorbance of the S-O band at 1020 cm^{-1} is identified as Ettringite (81).

The intensity of Si-O bonds in C_2S and C_3S reduces as C-S-H forms over time, and the absorbance bands observed at 823 cm^{-1} represent the vibrations of these bonds. Adding 20% BA to the HVFYA-SCC mix (CF70B20-R0) showed a significant decrement in the intensity of Si-O bonds as compared to HVFYA-SCC mix CF70B0-R0, indicating that BA and FYA increased the content of C-S-H after higher hydration age. The absorbance bands observed at 1257 cm^{-1} correspond to T-O-Si (T = tetrahedral Al and Si), which related to main hydration product of C-S-H (80, 82, 83). After a higher curing age, the BA and FYA compounds demonstrated higher pozzolanic activity and reacted with $Ca(OH)_2$, resulting in greater intensity in the T-O-Si band and important to developing more C-S-H. These results, visible in FTIR spectra, confirm the outcomes for compressive and shear strength.

3.3.3. Scanning electron microscopy

Various investigations have demonstrated that the mechanical characteristics of concrete are significantly influenced by the microstructure of the material (84, 85). This microstructure is affected by factors such as hydration time, cement type, water-cement ratio, and mineral admixtures (32, 86–89). The microstructure of concrete is comprised of the aggregate, interfacial transition zone (ITZ), and hydrated cement paste. In this study, SEM images of broken HVFYA-SCC specimens were taken in secondary electrons mode to investigate the microstructure.

The strength of concrete generally depends on the strength of the aggregates, porosity, source of collection of concrete debris, cement matrix, and ITZ between the matrix and the aggregates (19). Therefore, HVFA-SCC mixes made with higher replacement levels of RCA resulted in lower strength. Figure 13 and Figure 14 present the SEM images showing weak characteristics of RCA such as micro and macro pores, residual mortar/adhered mortar, cracks/fissures etc. Herein, the observed characteristics are certainly responsible for the overall poor structural behaviour of HVFA –SCC mixes (18, 19).

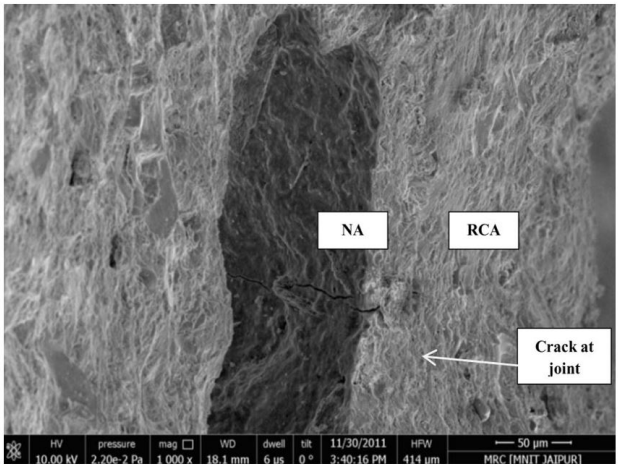

Figure 13. SEM image showing NCA and RCA [19].

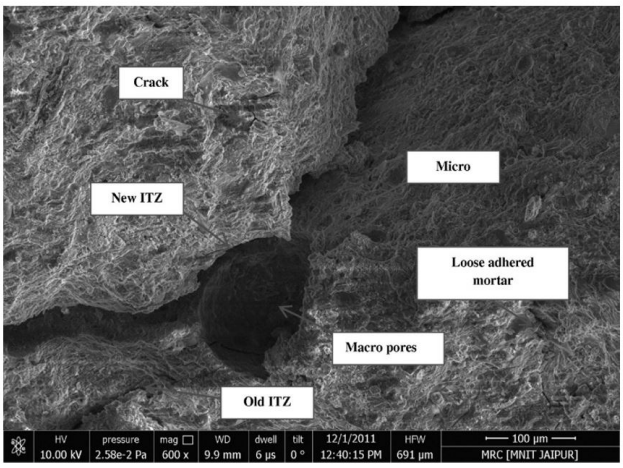

Figure 14. SEM image showing NCA and RCA based concrte [19].

The SEM images revealed that HVFYA-SCC mixes containing a higher content of BA had more microscopic air gaps, indicating their higher water-absorbing nature (24). Figure 15 (h-j) shows that voids grew and multiplied with 30% BA. Microstructure of HVFYA-SCC specimens with BA (30%) differed from that of the control HVFYA-SCC mix because of the slow pozzolanic activity of BA, which caused a slight reduction in compressive and shear strength behavior during the initial curing ages.

Simultaneously, the presence of BA further contributed in production of lower amount of C-S-H, consequently improving the microstructure of HVFYA-SCC mix. At initial ages, various irregular blocks and sheets were noticed for C-S-H, as the curing age continued for 120 days the irregular blocks were converted into dense crystals of C-S-H with rocky presence (Figure 15 (f)). As a result of dense and perfect development of C-S-H as identified in the images the resultant concrete matrix flaws were filled more efficiently leading towards better performance in term of shear and compressive strength (CF70B20-R25 mix) (Figure 15 (f)). Specific additional SEM images for the selected HVFYA-SCC mixes which are performing best and second best in comparison to the control HVFYA-SCC (CF70B0-R0) mix have also been incorporated to supplement the behaviour of HVFYA-SCC mixes (CF70B20-R25 & CF70B20-R0).

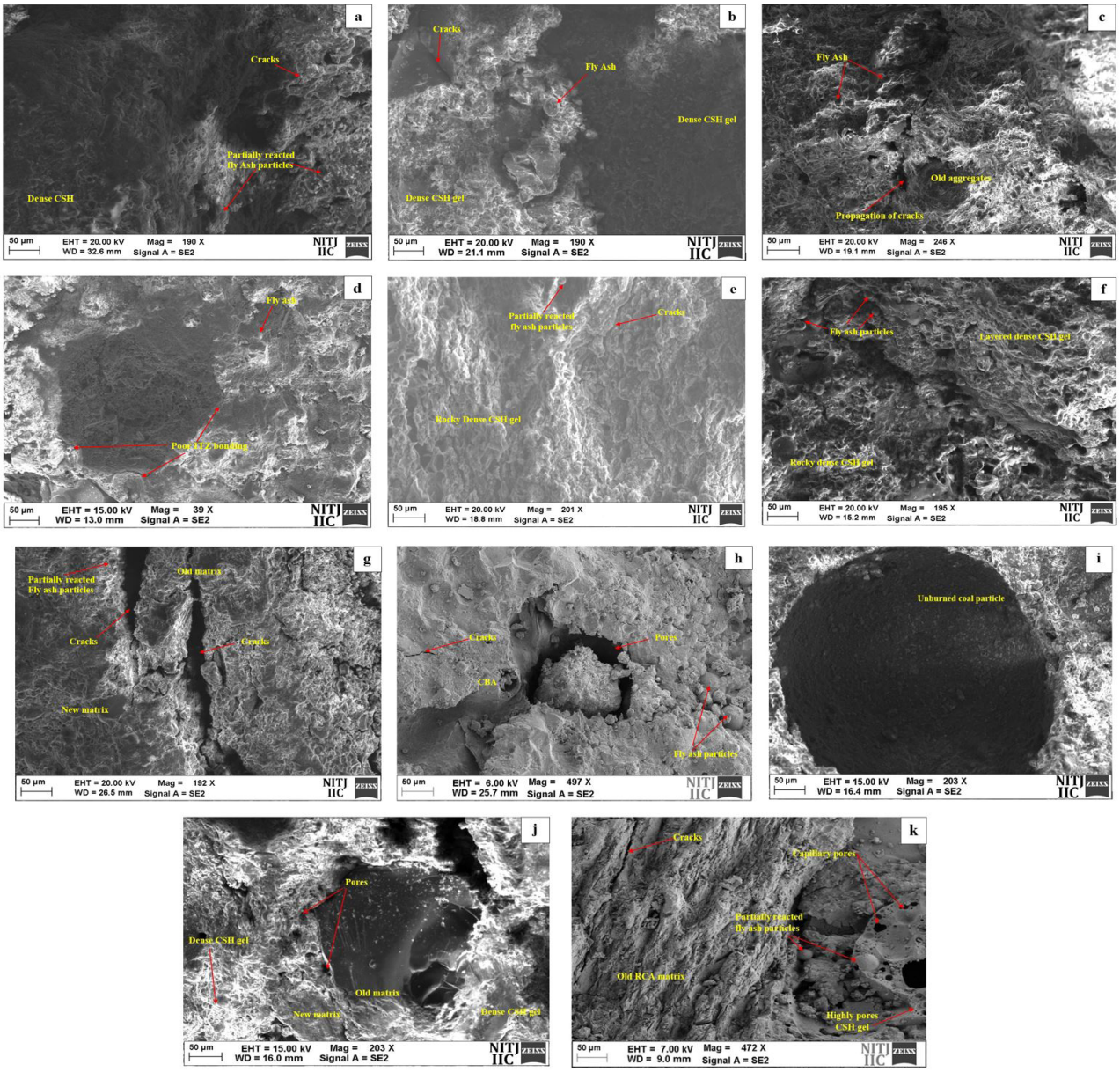

Figure 15. Microscopic images of HVFYA-SCC mixes at 120 days: (a) CF70B0-R0, (b) CF70B10-R0, (c) CF70B10-R25, (d) CF70B10-R50, (e) CF70B20-R0, (f) CF70B20-R25, (g) CF70B20-R50, (h-i) CF70B30-R0, (j) CF70B30-R25, (k) CF70B30-R50.

Further, it is important here to mention that the presence of C-S-H gel / crystals that are generally present in platy or hexagonal or in layered cloud form (s) are noticed at low magnification / scale. The clear differentiation of C-S-H crystals / gel can be noticed in Figure 16 (a-d).

Furthermore, Figure 15 (c-d), Figure 15 (g) and Figure 15 (j-k) for the HVFYA-SCC mixes CF70B10-R25, CF70B10-R50, CF70B20-R50, CF70B30-R25 and CF70B30-R50 present the concerns of presence of RCA (25% and 50%). The SEM images define weak bonding behavior due to presence of new and old mortar interfaces with clear boundaries. Since, the boundaries/ITZs' between the old and new mortar were weak in nature, resulting in significant drop in compressive and shear strength for the HVFYA-SCC mix CF70B10-R50, CF70B20-R50 and CF70B30-R50 in Figure 15 (d), Figure15 (g) and Figure 15 (k) respectively. Further, in Figure 15 (i) the unburnt coal particles were also spotted in SEM images for the HVFYA-SCC mixes with higher content of BA (30%). It has been confirmed from the literature that presence of unburnt carbon particles is a vital character of BA making it unsuitable for incorporation as an alternative of conventional aggregates in construction. Moreover, the larger quantities of unburned carbon particles adversely affect the hardened properties of mortars and concretes (90, 91). Figure 15 (h-k) furthermore indicate that the increasing the amount of BA (30%), beyond a certain percentage increase the overall porosity in the matrix due to higher water absorption (Table 3) leading towards weak microstructural performance.

3.4. Mathematical relationships

Linear regression analysis has established a correlation between mechanical characteristics and durability characteristics (92). Previous studies have reported R^2 values of 0.7, indicating a strong correlation among these characteristics (93, 94). Additionally, earlier research has suggested that fresh characteristics such as slump flow, T_{500}, V-funnel and L-box values exhibit a linear relationship with variation of BA in HVFYA-SCC mixes (58, 67, 95, 96). Figure 17(a) displays the outcomes of the present study, demonstrating a strong correlation amongst BA versus slump flow, with R^2 values of 0.9967, 0.9988 and 0.9979 with RCA variation. Similarly, T_{500} strongly correlates with BA with R^2 values above 0.9 (Figure

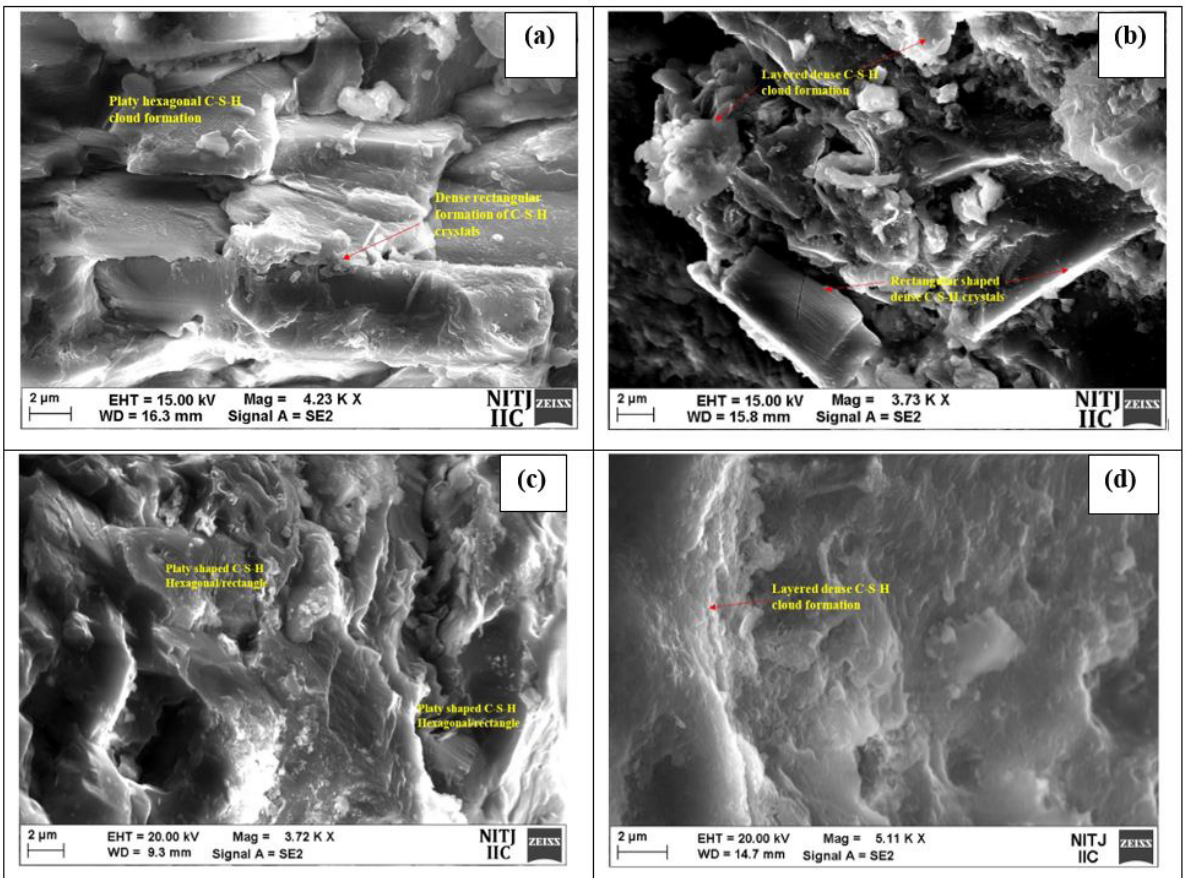

Figure 16. Microscopic images of HVFYA-SCC mixes at 120 days: (a) and (b) CF70B20-R25, (c) and (d) CF70B20-R0.

17(b)). Figures 17(c) & 17(d) showed a significant correlation between BA and V-funnel and L-box values respectively, with R^2 values higher than 0.9 (58, 67, 93). Figures 18 showed a significant correlation between compressive strength versus direct shear strength with R^2 values 0.9901 (93, 96, 97).

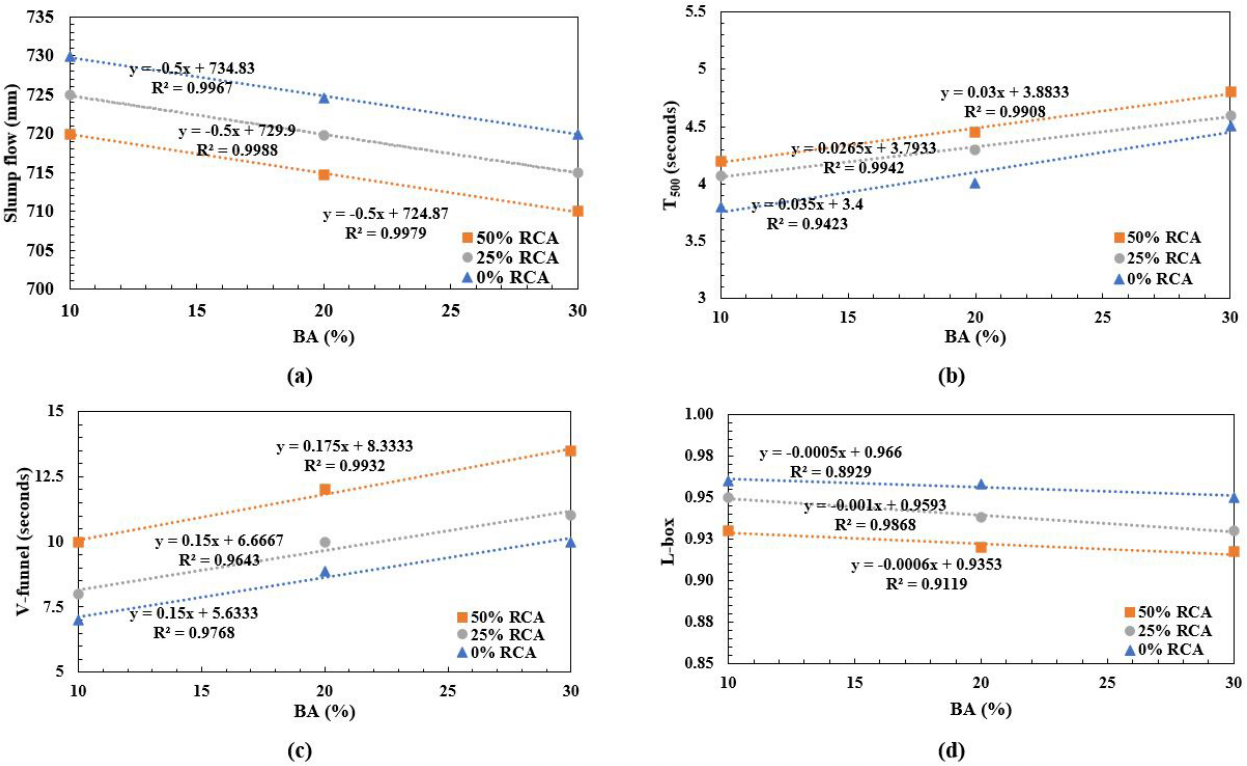

Figure 17. Coal bottom as (BA) versus: (a) slump flow, (b) T_{500}, (c) V-funnel, (d) L-box.

Table 5. Comparison of results with some previous studies.

Ref.	Types of concrete	FYA (%)	BA (%)	RCA (%)	water-to-binder (w/b) ratio	Compressive strength range (N/mm²)		Direct shear strength range (N/mm²)	
						28 Days	90 Days* / 120 Days#	28 Days	90 Days* / 120 Days#
(47)	HVFYA-SCC	30	-	50, 100	0.45	32.5-38.0	40-57.5#	-	-
(93)	HVFYA-SCC	40	-	-	0.26	32.5-45.0	40.0-55.0*	-	-
(31)	HVFYA-SCC	40	-	-	0.26	-	-	4.8-11.6	9.8-16.0*
(96)	HVFYA-SCC	50	-	50, 100	0.34	35.5-61.0	-	-	-
(106)	HVFYA-SCC	50	-	25, 50, 75, 100	0.38	23.5-54.0	-	-	-
(107)	HVFYA-SCC	50, 75	-	50, 100	0.35	7.17-53.45	-	-	-
(15)	HVFYA-SCC	30	10	25, 50, 75, 100	0.45	21.50-27.0	26.50-33.0*	-	-
(20)	HVFYA-SCC	50	10	25, 50, 75, 100	0.45	22-26.50	27-31.0	-	-
Present study	HVFYA-SCC	70	10, 20, 30	25, 50	0.25	24.30-34.44	45.51-51.26#	3.62-4.46	6.84-7.21#

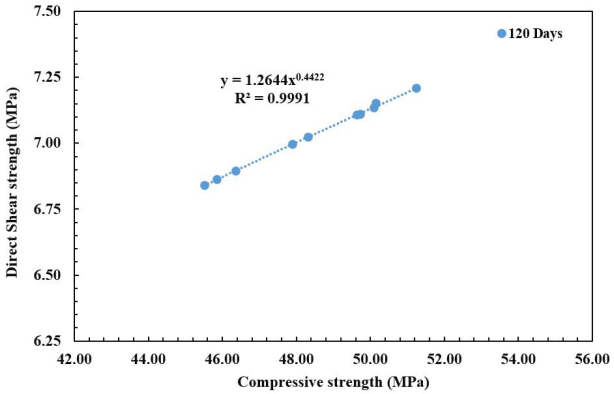

Figure 18. Relationship between compressive strength Vs direct shear strength.

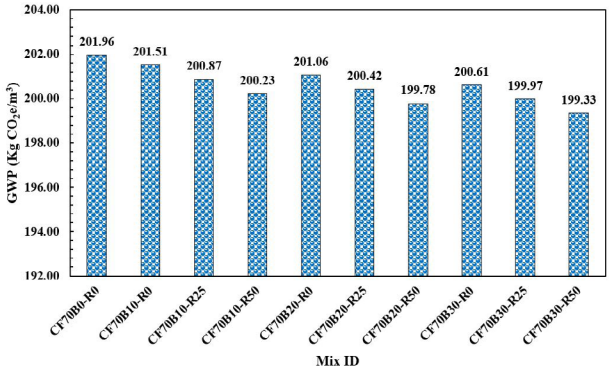

Figure 19. GWP values of HVFYA-SCC mixes per m^3.

Table 6. Embodied carbon dioxide of HVFYA-SCC mixes.

Materials	OPC	FYA	NFA	BA	NCA	RCA	SP	Water
Equivalent CO_2 (kg CO_2 e/m^3)	0.93	0.004	0.0014	0.00	0.0048	0.0012	0.0019	0.0008

It is worthwhile to mention that different authors have tested a wide range of parameters in their investigations. In this investigation, some previous studies have been selected and the considered parameters such as w/b and w/c ratio, curing period, range of compressive strength and shear strength are listed in Table 5 along with the parameters of the current investigation for comparison.

The shear strength reported previously and observed in the current study are also listed for reference. The authors are of the opinion that in such a situation, it is rather difficult to arrive at meaningful comparison.

3.5. Ecological evaluation of HVFYA-SCC mixes

There are several levers available in the literature to achieve the carbon neutrality such as carbon dioxide capture, utilization and storage (CCUS) (98), carbon capture and sequestration (CCS) (98), global warming potential (GWP) (93) etc. Out of these techniques, herein, the influence of RCA, CBA in HVFA-SCC mixes has been measured using the concept of GWP. GWP is a measure of how much energy the emissions of 1 ton of a gas will absorb over a given period of time, relative to the emissions of 1 ton of carbon dioxide (CO_2). The sustainability of concrete is usually determined through CO_2 emissions involved in producing the materials used for construction.

In the current study, GWP was analysed to assess the ecological influence of using different materials in HVFYA-SCC. GWP measures the greenhouse gases released in terms of CO_2 equivalent during the entire lifecycle of raw materials, from extraction to disposal (99). Various reliable sources were consulted to determine GWP, as presented in Table 6 (93, 99–103). The present investigate to compare the effects of using various materials in HVFYA-SCC mixes: NFA, BA, NCA, and RCA. The results (Figure 19) show that the HVFYA-SCC mix CF70B0-R0, which contained NFA (100%) and 100%, had the maximum carbon emission at 201.96 kgCO_2e/m^3. However, as the percentage of BA and RCA in other mixes increased, the carbon emission value declined. The HVFYA-SCC mix CF70B30-R50, with 30% BA and 50% RCA, had the lowest carbon emission value at 199.33 kgCO_2e/m^3. These findings suggest that incorporating BA up to 30% and RCA up to 50% with NFA and NCA in HVFYA-SCC mixes is more environmentally sustainable as these mixes release less CO_2 compared to control HVFYA-SCC mix (CF70B0-R0).

4. CONCLUSIONS

1. The workability of BA based HVFYA-SCC were negatively affected with an increase in RCA from 25% to 50%. This was attributed to the irregular BA particles and RCA, which increased friction and porosity ultimately decreasing the workability of mixes.
2. The compressive strength of the HVFYA-SCC mix CF70B20-R25 was approximately 7% more than the control HVFYA-SCC mix after 120 days. However, mix with 50% RCA resulted in inferior compressive strength.

3. The shear strength behavior of all BA based HVFYA-SCC mixes containing 25% RCA was lesser than the control HVFYA-SCC mix afterward 28 days. Though, after 120 days of curing, the shear strength of mix CF70B20-R25 was marginally higher than the control HVFYA-SCC mix. It has been concluded that additional pozzolanic reactions occurred due to presence of BA and FYA resulted in the formation of additional C-S-H thereby enhancing the shear strength of the HVFYA-SCC mixes.
4. FTIR analysis of HVFYA-SCC mix CF70B20-R25 confirmed that more amount of $Ca(OH)_2$ has been consumed after the 28 and 120 days curing period leading to an increase in the amount of C-S-H, as the intensity of the former has been decreased while that of later has been increased.
5. XRD analysis results confirmed that the Portlandite peak intensity decreased or disappeared and highest peaks of C-S-H in the HVFYA-SCC mix CF70B20-R25, after 120 days of curing indicating best compressive and shear strength values.
6. Analyzing the SEM images, it can be concluded that increasing amount BA > 20% reduces the overall strength due to increase in porosity and other weak physical characters. However, BA marginally contributes in the additional formation of C-S-H gel which is confirmed from FTIR and XRD results.
7. Incorporating RCA, reduces the overall strength due to weak bond among old and new mortar, and this behaviour become more severe with increase in the amount of RCA.
8. HVFA-SCC mix CF70B20-R25 resulted in good co-relation with compressive and shear strength (R^2 values 0.9901) Furthermore, the linear analysis also revealed a strong relationship amongst the BA and fresh properties.

The GWP has been calculated for all HVFYA-SCC mixes indicating lower values for the SCC mixes containing RCA and BA as compared to HVFYA-SCC mix made with natural ingredients. HVFYA-SCC mixes containing BA (10-30%) and RCA (25-50%) generate lower levels of CO_2 emissions than the control HVFYA-SCC mix (CF70B0-R0) by range of 0.22-1.30%.

Acknowledgments

The authors extend their appreciation to Dr. B.R. Ambedkar NIT Jalandhar, India and NITTTR, Chandigarh, India for granting access to research facilities and microstructural characterization.

Funding Sources

The first author expressed gratitude towards the Ministry of Education (MoE), Government of India, for providing financial aid as a scholarship during their PhD.

Authorship contribution statement

Amardeep Meena: Data cleansing, Formal analysis, Research, Methodology, Validation, Visualization, Write-up - original draft.

Navdeep Singh: Conceptualization, Data cleansing, Formal analysis, Research, Methodology, Project administration, Resources, Supervision, Validation, Visualization, Write-up - review & editing.

Surinder Pal Singh: Conceptualization, Formal analysis, Methodology, Project administration, Resources, Supervision, Validation, Visualization, Write-up - review & editing.

The authors of this article declare that they have no financial, professional or personal conflicts of interest that could have inappropriately influenced this work.

REFERENCES

1. Titiksh A, Wanjari SP. 2023. Predicting the strength of ultrahigh-volume ash concrete containing fly ash and bottom ash as a substitute for fine aggregates. J. Mater. Civ. Eng. 35(2):1–12. https://doi.org/10.1061/(ASCE)MT.1943-5533.0004573.
2. Chatterjee B. 2019. Demand for sand in urban India is 60mn metric tonnes per year: study. Hindustan Times. Retrieved from https://www.hindustantimes.com/cities/demand-for-sand-in-urban-india-is-60mn-metric-tonnes-per-year-study/story-wjl78UaUMeuTwXfrrz7DfN.html.
3. Parihar S. 2018. Supreme Court refuses to dilute ban on sand mining. India Today. Retrieved from https://www.indiatoday.in/india/story/supreme-court-refuses-to-dilute-ban-on-sand-mining-1313268-2018-08-13.
4. Singh A, Duan Z, Xiao J, Liu Q. 2020. Incorporating recycled aggregates in self-compacting concrete: a review. J. Sustain. Cem. Mater. 9(3):165–189. https://doi.org/10.1080/21650373.2019.1706205.
5. Singh N, Kumar P, Goyal P. 2019. Reviewing the behaviour of high volume fly ash based self compacting concrete. J. Build. Eng. 26:100882. https://doi.org/10.1016/j.jobe.2019.100882.
6. Tuyan M, Mardani-Aghabaglou A, Ramyar K. 2014. Freeze-thaw resistance, mechanical and transport properties of self-consolidating concrete incorporating coarse recycled concrete aggregate. Mater. Des. 53:983-991. https://doi.org/10.1016/j.matdes.2013.07.100.
7. Aggarwal Y, Siddique R. 2014. Microstructure and properties of concrete using bottom ash and waste foundry sand as partial replacement of fine aggregates. Constr. Build. Mater. 54:210–233. https://doi.org/10.1016/j.conbuildmat.2013.12.051.
8. Singh M, Siddique R. 2016. Effect of coal bottom ash as partial replacement of sand on workability and strength properties of concrete. J. Clean. Prod. 112:620–630. https://doi.org/10.1016/j.jclepro.2015.08.001.
9. Rashad AM. 2014. A comprehensive overview about the influence of different admixtures and additives on the properties of alkali-activated fly ash. Mater. Des. 53:1005–1025. https://doi.org/10.1016/j.matdes.2013.07.074.
10. Wu Y, Lu B, Bai T, Wang H, Du F, Zhang Y. et al. 2019. Geopolymer, green alkali activated cementitious material: Synthesis, applications and challenges. Constr. Build. Mater. 224:930–49.https://doi.org/10.1016/j.conbuildmat.2019.07.112.
11. Rathee M, Singh N. 2022. Durability properties of copper slag and coal bottom ash based I-shaped geopolymer paver blocks. Constr. Build. Mater. 347:128461. https://doi.

org/10.1016/j.conbuildmat.2022.128461.
12. Sanjuán MÁ, Andrade C, Mora P, Zaragoza A. 2020. Carbon dioxide uptake by cement-based materials: A spanish case study. Appl. Sci. 10(1):339. https://doi.org/10.3390/app10010339.
13. Volz JS. 2012. High-volume fly ash concrete for sustainable construction. Adv. Mater. Res. 512–515:2976–81. https://doi.org/10.4028/www.scientific.net/AMR.512-515.2976.
14. Malhotra VM, Mehta PK. 2008. High-performance, high-volume fly ash concrete. in: 3rd supple. cement. Mater. for Sust. Devel. Inc., Ottawa, Canada. 142.
15. Singh N, Mithulraj M, Arya S. 2019. Utilization of coal bottom ash in recycled concrete aggregates based self compacting concrete blended with metakaolin. Resour. Conserv. Recycl. 144:240–251. https://doi.org/10.1016/j.resconrec.2019.01.044.
16. Meena A, Singh N, Singh SP. 2022. Mechanical properties of polypropylene fiber-reinforced geopolymer composites: a review. In: Laishram, B., Tawalare, A. (eds) Recent Advancements in Civil Engineering. ACE 2020. Lecture Notes in Civil Engineering, 172. Springer, Singapore. https://doi.org/10.1007/978-981-16-4396-5_24.
17. Singh N, Singh SP. 2016. Carbonation resistance and microstructural analysis of low and high volume fly ash self compacting concrete containing recycled concrete aggregates. Constr. Build. Mater. 127:828–842. https://doi.org/10.1016/j.conbuildmat.2016.10.067.
18. Kapoor K, Singh SP, Singh B. 2017. Permeability of self-compacting concrete made with recycled concrete aggregates and metakaolin. J. Sustain. Cem. Mater. 6(5):293–313. https://doi.org/10.1080/21650373.2017.1280426.
19. Singh N, Singh SP. 2018. Validation of carbonation behavior of self compacting concrete made with recycled aggregates using microstructural and crystallization investigations. Eur. J. Environ. Civ. Eng. 24(13):2187-2210. https://doi.org/10.1080/19648189.2018.1500312.
20. Kumar P, Singh N. 2020. Influence of recycled concrete aggregates and coal bottom ash on various properties of high volume fly ash-self compacting concrete. J. Build. Eng. 32:101491. https://doi.org/10.1016/j.jobe.2020.101491.
21. Singh N, Shehnazdeep, Bhardwaj A. 2020. Reviewing the role of coal bottom ash as an alternative of cement. Constr. Build. Mater. 233:117276. https://doi.org/10.1016/j.conbuildmat.2019.117276.
22. Siddique R, Kunal. 2015. Design and development of self-compacting concrete made with coal bottom ash. J. Sustain. Cem. Mater. 4(3-4):225–237. https://doi.org/10.1080/21650373.2015.1004138.
23. Siddique R, Aggarwal P, Aggarwal Y. 2012. Influence of water/powder ratio on strength properties of self-compacting concrete containing coal fly ash and bottom ash. Constr. Build. Mater. 29:73–81. https://doi.org/10.1016/j.conbuildmat.2011.10.035.
24. Zainal Abidin NE, Wan Ibrahim MH, Jamaluddin N, Kamaruddin K, Hamzah AF. 2014. The effect of bottom ash on fresh characteristic, compressive strength and water absorption of self-compacting concrete. Appl. Mech. Mater. 660:145–151. https://doi.org/10.4028/www.scientific.net/AMM.660.145.
25. Xiao J, Xie H, Yang Z. 2012. Shear transfer across a crack in recycled aggregate concrete. Cem. Concr. Res. 42(5):700–709. https://doi.org/10.1016/j.cemconres.2012.02.006.
26. Waseem SA, Singh B. 2016. Shear transfer strength of normal and high-strength recycled aggregate concrete – An experimental investigation. Constr. Build. Mater. 125:29–40. https://doi.org/10.1016/j.conbuildmat.2016.08.022.
27. Rahal KN, Alrefaei YT. 2017. Shear strength of longitudinally reinforced recycled aggregate concrete beams. Eng. Struct. 145:273–282. https://doi.org/10.1016/j.engstruct.2017.05.028.
28. Li Y, Zhou Y, Wang R, Li Y, Wu X, Si Z. 2022. Experimental investigation on the properties of the interface between RCC layers subjected to early-age frost damage. Cem. Concr. Compos. 134:104745. https://doi.org/10.1016/j.cemconcomp.2022.104745.
29. Rahal K. 2017. Shear strength of recycled aggregates concrete. Procedia. Eng. 210:105–108. https://doi.org/10.1016/j.proeng.2017.11.054.
30. Sadati S, Arezoumandi M, Khayat KH, Volz JS. 2016. Shear performance of reinforced concrete beams incorporating recycled concrete aggregate and high-volume fly ash. J. Clean. Prod. 115:284–293. https://doi.org/10.1016/j.jclepro.2015.12.017.
31. Simalti A, Singh AP. 2020. Comparative study on direct shear behavior of manufactured and recycled shredded tyre steel fiber reinforced self-consolidating concrete. J. Build. Eng. 29:101169. https://doi.org/10.1016/j.jobe.2020.101169.
32. Meena A, Singh N, Singh SP. 2023. High-volume fly ash Self consolidating concrete with coal bottom ash and recycled concrete aggregates: fresh, mechanical and microstructural properties. J. Build. Eng. 63:105447. https://doi.org/10.1016/j.jobe.2022.105447.
33. Curpen S, Teutsch N, Kovler K, Spatari S. 2023. Evaluating life cycle environmental impacts of coal fly ash utilization in embankment versus sand and landfilling. J. Clean. Prod. 385:135402. https://doi.org/10.1016/j.jclepro.2022.135402.
34. Mocharla IR, Selvam R, Govindaraj V, Muthu M. 2022. Performance and life-cycle assessment of high-volume fly ash concrete mixes containing steel slag sand. Constr. Build. Mater. 341:127814. https://doi.org/10.1016/j.conbuildmat.2022.127814.
35. Rathnayake M, Julnipitawong P, Tangtermsirikul S, Toochinda P. 2018. Utilization of coal fly ash and bottom ash as solid sorbents for sulfur dioxide reduction from coal fired power plant: Life cycle assessment and applications. J. Clean. Prod. 202:934–945. https://doi.org/10.1016/j.jclepro.2018.08.204.
36. Liu Z, Chin CS, Xia J, Lu J, Wang X. 2023. Exploring the sustainability of concrete with fly ash, recycled coarse aggregate and biomineralisation method by life cycle assessment. J. Clean. Prod. 406:137077. https://doi.org/10.1016/j.jclepro.2023.137077.
37. Chen X, Wang H. 2022. Life-cycle assessment and multi-criteria performance evaluation of pervious concrete pavement with fly ash. Resour. Conserv. Recycl. 177:105969. https://doi.org/10.1016/j.resconrec.2021.105969.
38. Du J, Liu Z, Christodoulatos C, Conway M, Bao Y, Meng W. 2022. Utilization of off-specification fly ash in preparing Ultra-High-Performance Concrete (UHPC): Mixture design, characterization, and life-cycle assessment. Resour. Conserv. Recycl. 180:106136. https://doi.org/10.1016/j.resconrec.2021.106136.
39. Das P, Cheela VRS, Mistri A, Chakraborty S, Dubey B, Barai SV. 2022. Performance assessment and life cycle analysis of concrete containing ferrochrome slag and fly ash as replacement materials – A circular approach. Constr. Build. Mater. 347:128609. https://doi.org/10.1016/j.conbuildmat.2022.128609.
40. IS: 8112. 2013. Ordinary portland cement, 43 grade-specification. Bur. Indian Stand. New Delhi, India. 1-17.
41. ASTM C 618. 2014. Standard specification for coal fly ash and raw or calcined natural pozzolan for use in concrete. 1–5.
42. IS:383. 2016. Indian Standard coarse and fine aggregate for concrete- specification. Bur. Indian Stand. New Delhi, India. 1–21.
43. IRC:121. 2017. Guidelines for use of construction and demolition waste in road sector. Indian Road Congress. 1:1-28.
44. Jamaluddin N, Hamzah AF, Wan Ibrahim MH, Jaya RP, Arshad MF, Abidin NEZ. et al. 2016. Fresh properties and flexural strength of self-compacting concrete integrating coal bottom ash. in. MATEC Web Conf. 47:1–6.
45. Siddique R, Aggarwal P, Aggarwal Y. 2012. Mechanical and durability properties of self-compacting concrete containing fly ash and bottom ash. J. Sustain. Cem. Mater. 1(3):67–82. https://doi.org/10.1080/21650373.2012.726820.
46. Singh N, Nassar RUD, Shehnazdeep K, Anjani B. 2022. Microstructural characteristics and carbonation resistance of coal bottom ash based concrete mixtures. Mag. Concr. Res. 74:364–378. https://doi.org/10.1680/jmacr.20.00125.
47. Kapoor K, Singh SP, Singh B. 2016. Durability of self-compacting concrete made with recycled concrete aggregates and mineral admixtures. Constr. Build. Mater. 128:67–76. https://doi.org/10.1016/j.conbuildmat.2016.10.026.
48. Chiranjiakumari Devi S, Ahmad Khan R. 2020. Influence of graphene oxide on sulfate attack and carbonation of concrete

containing recycled concrete aggregate. Constr. Build. Mater. 250:118883. https://doi.org/10.1016/j.conbuildmat.2020.118883.
49. Singh M, Siddique R. 2014. Compressive strength, drying shrinkage and chemical resistance of concrete incorporating coal bottom ash as partial or total replacement of sand. Constr. Build. Mater. 68:39–48. https://doi.org/10.1016/j.conbuildmat.2014.06.034.
50. IS 9103. 1999. Specification for concrete admixtures. Bur. Indian Stand. New Delhi, India. 1–22.
51. EFNARC. 2005. The european guidelines for self-compacting concrete specification, production and use. 1-68.
52. IS 516. Hardened concrete- methods of test, part 1: testing of strength of hardened concrete. Bur. Indian Stand. New Delhi, India.
53. Bairagi NK, Modhera CD. 2001. Shear strength of fibre reinforced concrete. Indian Concr. Inst. J. 1(4):47–52.
54. Jain A, Chaudhary S, Gupta R. 2022. Mechanical and microstructural characterization of fly ash blended self-compacting concrete containing granite waste. Constr. Build. Mater. 314:125480. https://doi.org/10.1016/j.conbuildmat.2021.125480.
55. Singh N, Arya S, Mithul Raj M. 2019. Assessing the performance of self-compacting concrete made with recycled concrete aggregates and coal bottom ash using ultrasonic pulse velocity. In: Agnihotri, A., Reddy, K., Bansal, A. (eds) Recycled waste materials. Lecture notes in civil engineering, 32. Springer, Singapore. https://doi.org/10.1007/978-981-13-7017-5_19.
56. Martínez-García R, Guerra-Romero IM, Morán-del Pozo JM, De Brito J, Juan-Valdés A. 2020. Recycling aggregates for self-compacting concrete production: A feasible option. Materials 13(4):868. https://doi.org/10.3390/ma13040868.
57. Tuyan M, Mardani-Aghabaglou A, Ramyar K. 2014. Freeze-thaw resistance, mechanical and transport properties of self-consolidating concrete incorporating coarse recycled concrete aggregate. Mater. Des. 53:983–991. https://doi.org/10.1016/j.matdes.2013.07.100.
58. Rafieizonooz M, Mirza J, Salim MR, Hussin MW, Khankhaje E. 2016. Investigation of coal bottom ash and fly ash in concrete as replacement for sand and cement. Constr. Build Mater. 116:15–24. https://doi.org/10.1016/j.conbuildmat.2016.04.080.
59. Sanjuán MA, Argiz C. 2016. Coal fly ash alkalis content characterization by means of a full factorial design. Mater. Lett. 164:528–531. https://doi.org/10.1016/j.matlet.2015.11.034.
60. Allahverdi A, Shaverdi B, Kani EN. 2010. Influence of sodium oxide on properties of fresh and hardened paste of alkali-activated blast-furnace slag. Int. J. Civ. Eng. 8(4):304–14.
61. Shukla A. 2020. Effect of sodium oxide on physical and mechanical properties of fly-ash based geopolymer composites. Indian J. Sci. Technol. 13(38):3994–4002. https://doi.org/10.17485/IJST/v13i38.1663.
62. Zhang J, Shi C, Zhang Z. 2021. Effect of Na_2O concentration and water/binder ratio on carbonation of alkali-activated slag/fly ash cements. Constr. Build. Mater. 269:121258. https://doi.org/10.1016/j.conbuildmat.2020.121258.
63. Santos TA, Neto JSA, Cilla MS, Ribeiro DV. 2022. Influence of the content of alkalis (Na_2O and K_2O), MgO, and SO_3 present in the granite rock fine in the production of portland clinker. J. Mater. Civ. Eng. 34(3):1–12. https://doi.org/10.1061/(ASCE)MT.1943-5533.0004201.
64. De Pádua PGL, Cordeiro GC. 2021. Effect of K_2O content on properties of sugar cane bagasse ash-cement-based systems. Adv. Cem. Res. 34(2):57–66. https://doi.org/10.1680/jadcr.20.00082.
65. Kurda R, de Brito J, Silvestre JD. 2017. Influence of recycled aggregates and high contents of fly ash on concrete fresh properties. Cem. Concr. Compos. J. 84:198–213. https://doi.org/10.1016/j.cemconcomp.2017.09.009.
66. India Today. 2018. Indian coal reserves: classification of coal and where it is found in the country. India Today Web Desk, New Delhi, India. Retrieved from https://www.indiatoday.in/education-today/gk-current-affairs/story/indian-coal-reserves-classification-of-coal-and-where-it-is-found-in-the-country-1338928-2018-09-13.
67. Majhi RK, Nayak AN. 2019. Properties of concrete incorporating coal fly ash and coal bottom ash. J. Inst. Eng. India Ser. A. 100:459–469. https://doi.org/10.1007/s40030-019-00374-y.
68. Singh N, Singh SP. 2016. Carbonation and electrical resistance of self compacting concrete made with recycled concrete aggregates and metakaolin. Constr. Build. Mater. 121:400–409. https://doi.org/10.1016/j.conbuildmat.2016.06.009.
69. Singh M, Siddique R, Ait-Mokhtar K, Belarbi R. 2015. Durability properties of concrete made with high volumes of low-calcium coal bottom ash as a replacement of two types of sand. J. Mater. Civ. Eng. 28(4):04015175. https://doi.org/10.1061/(ASCE)MT.1943-5533.0001464.
70. Wilben S, Supit M, Uddin F, Shaikh A. 2015. Durability properties of high volume fly ash concrete containing nano-silica. Mater. Struct. 48:2431–2445. https://doi.org/10.1617/s11527-014-0329-0.
71. Sun J, Shen X, Tan G, Tanner JE. 2019. Modification effects of Nano-SiO_2 on early compressive strength and hydration characteristics of high-volume fly ash concrete. J. Mater. Civ. Eng. 31(6):1–12. https://doi.org/10.1061/(ASCE)MT.1943-5533.0002665.
72. Jindal BB. 2018. Feasibility study of ambient cured geopolymer concrete - a review. Adv. Concr. Constr. 6(4):387–405. https://doi.org/10.12989/acc.2018.6.4.387.
73. Devi SC, Khan RA. 2020. Effect of sulfate attack and carbonation in graphene oxide–reinforced concrete containing recycled concrete aggregate. J. Mater. Civ. Eng. 32(11):04020339. https://doi.org/10.1061/(ASCE)MT.1943-5533.0003415.
74. Timakul P, Rattanaprasit W, Aungkavattana P. 2016. Improving compressive strength of fly ash-based geopolymer composites by basalt fibers addition. Ceram. Int. 42(5):6288–6295. https://doi.org/10.1016/j.ceramint.2016.01.014.
75. Jain A, Gupta R, Chaudhary S. 2019. Performance of self-compacting concrete comprising granite cutting waste as fine aggregate. Constr. Build. Mater. 221:539–552. https://doi.org/10.1016/j.conbuildmat.2019.06.104.
76. Cheng R, Gen M, Tsujimura Y. 1996. A tutorial survey of job-shop scheduling problems using genetic algorithms - I. Representation. Comput. Ind. Eng. 30(4):983–997. https://doi.org/10.1016/0360-8352(96)00047-2.
77. Bhatrola K, Kothiyal NC. 2023. Comparative study of physico-mechanical performance of PPC mortar incorporated 1D/2D functionalized nanomaterials. Int. J. Appl. Ceram. Technol. 20(4):2478–2498. https://ceramics.onlinelibrary.wiley.com/doi/abs/10.1111/ijac.14372.
78. Biricik H, Sarier N. 2014. Comparative study of the characteristics of nano silica-, silica fume- and fly ash-incorporated cement mortars. Mater. Res. 17(3):570–582. https://doi.org/10.1590/S1516-14392014005000054.
79. Bhatrola K, Kothiyal NC. 2023. Influence of (1D/2D) hybrid nanomaterials on the mechanical and durability properties of pozzolana portland cementitious mortar. J. Adhes. Sci. Technol. 1–25. https://doi.org/10.1080/01694243.2023.2226287.
80. Lo FC, Lee MG, Lo SL. 2021. Effect of coal ash and rice husk ash partial replacement in ordinary Portland cement on pervious concrete. Constr. Build. Mater. 286:122947. https://doi.org/10.1016/j.conbuildmat.2021.122947.
81. Ylmén R, Jäglid U, Steenari BM, Panas I. 2009. Early hydration and setting of Portland cement monitored by IR, SEM and Vicat techniques. Cem. Concr. Res. 39(5):433–439. https://doi.org/10.1016/j.cemconres.2009.01.017.
82. Lee TC, Rao MK. 2009. Recycling municipal incinerator fly- and scrubber-ash into fused slag for the substantial replacement of cement in cement-mortars. Waste Manag. 29(6):1952–1959. https://doi.org/10.1016/j.wasman.2009.01.002.
83. Maurya SK, Kothiyal NC. 2023. Effect of graphene oxide and functionalized carbon nanotubes on mechanical and durability properties of high volume fly-ash cement nanocomposite. Eur. J. Environ. Civ. Eng. 1–17. https://doi.org/10.1080/19648189.2023.2229401.
84. Sharma R, Khan RA. 2017. Sustainable use of copper slag in self compacting concrete containing supplementary cementitious materials. J. Clean. Prod. 151:179–192. https://doi.org/10.1016/j.jclepro.2017.03.031.
85. Singh N, Singh SP. 2016. Carbonation resistance and microstructural analysis of low and high volume fly ash self compacting concrete containing recycled concrete

aggregates. Constr. Build. Mater. 127:828–842. https://doi.org/10.1016/j.conbuildmat.2016.10.067.
86. Siddique R. 2013. Compressive strength, water absorption, sorptivity, abrasion resistance and permeability of self-compacting concrete containing coal bottom ash. Constr. Build. Mater. 47:1444–1450. https://doi.org/10.1016/j.conbuildmat.2013.06.081.
87. Gooi S, Mousa AA, Kong D. 2020. A critical review and gap analysis on the use of coal bottom ash as a substitute constituent in concrete. J. Clean. Prod. 268:121752. https://doi.org/10.1016/j.jclepro.2020.121752.
88. Singh M, Siddique R. 2014. Strength properties and micro-structural properties of concrete containing coal bottom ash as partial replacement of fine aggregate. Constr. Build. Mater. 50:246–256. https://doi.org/10.1016/j.conbuildmat.2013.09.026.
89. Akhil, Singh N. 2024. Microstructural characteristics of iron-steel slag concrete : A brief review. Mater. Today Proc. https://doi.org/10.1016/j.matpr.2023.03.548.
90. Ha TH, Muralidharan S, Bae JH, Ha YC, Lee HG, Park KW, Kim DK. 2005. Effect of unburnt carbon on the corrosion performance of fly ash cement mortar. Constr. Build. Mater. 19(7):509–515. https://doi.org/10.1016/j.conbuildmat.2005.01.005.
91. Lv B, Jiao F, Chen Z, Dong B, Fang C, Zhang C, Deng X. 2022. Separation of unburned carbon from coal fly ash: Pre-classification in liquid–solid fluidized beds and subsequent flotation. Process Saf. Environ. Prot. 165:408–419. https://doi.org/10.1016/j.psep.2022.07.031.
92. Nassar RUD, Singh N, Varsha S, Sai AR, Sufyan-Ud-Din M. 2022. Strength, electrical resistivity and sulfate attack resistance of blended mortars produced with agriculture waste ashes. Case. Stud. Constr. Mater. 16:e00944. https://doi.org/10.1016/j.cscm.2022.e00944.
93. Simalti A, Singh AP. 2021. Comparative study on performance of manufactured steel fiber and shredded tire recycled steel fiber reinforced self-consolidating concrete. Constr. Build. Mater. 266(Part B):121102. https://doi.org/10.1016/j.conbuildmat.2020.121102.
94. Mastali M, Dalvand A. 2016. Use of silica fume and recycled steel fibers in self-compacting concrete (SCC). Constr. Build. Mater. 125:196–209. https://doi.org/10.1016/j.conbuildmat.2016.08.046.
95. Sukumar B, Nagamani K, Srinivasa Raghavan R. 2008. Evaluation of strength at early ages of self-compacting concrete with high volume fly ash. Constr. Build. Mater. 22(7):1394–1401. https://doi.org/10.1016/j.conbuildmat.2007.04.005.
96. Singh RB, Debbarma S, Kumar N, Singh S. 2021. Hardened state behaviour of self-compacting concrete pavement mixes containing alternative aggregates and secondary binders. Constr. Build. Mater. 266(Part A):120624. https://doi.org/10.1016/j.conbuildmat.2020.120624.
97. Sahmaran M, Yaman IO, Tokyay M. 2009. Transport and mechanical properties of self consolidating concrete with high volume fly ash. Cem. Concr. Compos. 31(2):99–106. https://doi.org/10.1016/j.cemconcomp.2008.12.003.
98. Sanjuán MA, Argiz C, Mora P, Zaragoza A. 2020. Carbon dioxide uptake in the roadmap 2050 of the spanish cement industry. Energies. 13(13):3452. https://doi.org/10.3390/en13133452.
99. Sharma R, Senthil K. 2023. An investigation on mechanical and microstructural properties of hybrid fiber reinforced concrete with manufactured sand and recycled coarse aggregate. J. Build. Eng. 69:106236. https://doi.org/10.1016/j.jobe.2023.106236.
100. Kurad R, Silvestre JD, De Brito J, Ahmed H. 2017. Effect of incorporation of high volume of recycled concrete aggregates and fly ash on the strength and global warming potential of concrete. J. Clean. Prod. 166:485–502. https://doi.org/10.1016/j.jclepro.2017.07.236.
101. Devi SC, Khan RA. 2020. Compressive strength and durability behavior of graphene oxide reinforced concrete composites containing recycled concrete aggregate. J. Build. Eng. 32:101800. https://doi.org/10.1016/j.jobe.2020.101800.
102. Mastali M, Dalvand A, Sattarifard AR, Illikainen M. 2018. Development of eco-efficient and cost-effective reinforced self-consolidation concretes with hybrid industrial/recycled steel fibers. Constr. Build. Mater. 166:214–226. https://doi.org/10.1016/j.conbuildmat.2018.01.147.
103. Pavlu T, Kocí V, Hájek P. 2019. Environmental assessment of two use cycles of recycled aggregate concrete. Sustain. 11(21):6185. https://doi.org/10.3390/su11216185.
104. IS 269. 2015. Requirements of ordinary portland cement. Bur. Indian Stand. New Delhi, India.
105. IS: 4031 (Part 6). 1988. Determination of compressive strength of hydraulic cement other than masonary cement. Bur. Indian Stand. New Delhi, India. 1-11.
106. Khodair Y, Bommareddy B. 2017. Self-consolidating concrete using recycled concrete aggregate and high volume of fly ash, and slag. Constr. Build. Mater. 153:307–316. https://doi.org/10.1016/j.conbuildmat.2017.07.063.
107. Guo Z, Jiang T, Zhang J, Kong X, Chen C, Lehman DE. 2020. Mechanical and durability properties of sustainable self-compacting concrete with recycled concrete aggregate and fly ash, slag and silica fume. Constr. Build. Mater. 231:117115. https://doi.org/10.1016/j.conbuildmat.2019.117115.